

We thank reviewer for acknowledging the impact of this paper and their comments which we have discussed below and think have significantly improved the manuscript.

2.1 I think this article's first and foremost improvement point is that the research goal is not clear and in-depth enough.

We apologise for a lack of clarity here, and agree that the twin goals of methodology comparison and ecological insight are not presented in as clear a manner as they could be. We have edited the wording in section 1.3 to improve their readability and enhance the communication of their importance (L132-133):

"The aims of this study are twofold: the first aim is to compare three TLS methods for estimating PAI with traditional DHP. The second aim of this study is to use TLS to understand drivers of individual tree a variation."

2.2 The presentation of the results is not complete, which makes it difficult for readers to capture their needed information, such as the WAI variation trend (functions) among 5 tree species related to their height and density.

We apologise that our analysis of WAI was not clear to the reviewer. We chose to compare methods based on PAI estimates, and not WAI or LAI, to avoid introducing additional processing steps and complexity and therefore to more directly compare the chosen methodological approaches. Differences in PAI between different TLS and DHP estimates can be attributed to differences in processing approaches, whereas comparison of WAI introduces additional error from separation approaches.

To improve clarity, we have added the following (L241-242):

"We chose to compare PAI values rather than WAI or LAI as each method corrects for non-photosynthetic elements in different ways and would introduce bias, limiting the ability to directly compare metrics."

See also our response to comment 2.4 below.

2.3 Referring to the DHP results, authors evaluated the error of WAI and PAI analyzed by point clouds. I would like to know if the authors use the TLS data to improve the LAI evaluation accuracy. TLS can support assessing the single tree and plot-level WAI more accurately.

We agree completely that the combination of TLS and DHP might improve analyses, and this has been developed in methods not tested in this paper (e.g. Kamoske et al., 2019).

Here we did not use the two datasets together, preferring instead to retain the ability to compare them as independent estimates of the indices of interest. We note that neither should be viewed as the 'truth', and therefore using them in combination could introduce additional biases that would be challenging to disentangle. Nevertheless, others could use our data to perform the analyses suggested.

2.4 More importantly, whether the WAI of different Mediterranean trees has similarities between the same species, as well as providing specific information (maybe list in thematic tables to show the relationship among species, tree height, density, and PAI), will make readers benefit greatly. I think the measured data of this study can

support this research goal, while they are not fully presented in the current edition.

Although these are not the focus of this study, we agree that additional information could prove useful to some readers. We thank the reviewer for their suggestion of including WAI analysis, which we think has significantly improved the manuscript. We have added Figure C2 and Tables C3, C4 to the supplementary information and refer to this in the main manuscript, section 3.4 (L320 – 322):

"To understand drivers of variance in WAI we carried out additional analysis to test the relationship between WAI and species, height, CAI and PAI, and presented these results in Appendix C."

2.5 In addition, the presentation of the results is incomplete. I did not find the location, site conditions and tree species appearance of the measured plots shown in the manuscript.

We apologise for this omission. This information is presented in the cited study Owen et al. (2021), but we have added a detailed site map to the supplementary materials, Figure B1, which is referred to in L145 of the main text.

Please see also our response to comment 2.14

2.6 The segmentation results of different tree species and the statistical information on PAI and WAI of trees grown in different site conditions were also not provided.

We thank the reviewer for their comment and apologise for lack of clarity around the segmentation process. Individual tree segmentation was carried out by the authors for a separate study (Owen et al., 2021). We have amended section 2.5 (L218 – 222) to clarify the segmentation process and have signposted (Owen et al., 2021).

Please see also our response to comment 2.17.

2.7 In addition, critical mathematical functions and quantitative conclusions are also lacking in the current edition.

We apologise for this lack of completeness. We are not entirely clear to which functions the reviewer refers, but for reasons of clarity and brevity we chose to primarily describe the various processing methods we used rather than repeat their original descriptions, which are extensive within the cited literature. Where equations have been used from other studies, we have cited the original equation number along with the paper in-text (but see response to 2.8 below).

2.8 I suggest authors reconsider whether it is necessary to study the CAI. This parameter can be easily analyzed using remote sensing images without using TLS.

In this study we used CAI as a proxy measure of stand density (L248), which was a necessary within our model to both understand and correct for the effect of stand density on wood to plant ratio, α . Controlling for stand density (using CAI as a proxy) is important as trees growing in dense plots have lower water availability per tree (see L75-77). We chose to use CAI as Owen et al., (2021) showed that the metric is also indicative of plot-level competition and the metric accounts for crown overlap which cannot be estimated from

imagery in closed forests. Furthermore, Coomes et al., (2012) showed CAI to be better than traditional metrics such as basal area, as it is more intuitive to non-specialists and strongly predicts productivity.

We apologise for the lack of clarity when describing this metric and its intended use in the study, which was also commented on by reviewer 1 (comment 1.7).

We have therefore amended our description of the key metric, CAI, for quantifying stand density and local competition in section 2.6 L245-248:

"To further understand observed drivers of variance in PAI, we tested the relationship between PAI and TLS estimated whole plot crown area index, CAI, calculated as the sum of projected crown area divided by the plot area (Owen et al., 2021), and a proxy measure of stand density and local competition (Caspersen et al., 2011; Coomes et al., 2012), using SMA."

2.9 Furthermore, is it applicable to use a fixed voxel size when analyzing WAI? After all, different tree species have various canopy shapes and branch structure features. Adaptive adjusting the voxel size according to the point cloud density and the branch distribution trend may be more reasonable.

We thank the reviewer for their comment on voxel size and agree that finding an appropriate voxel size a complex problem (discussed extensively in the response to the other reviewer). We chose the method of voxel classification rather than a radiative transfer approach as it has a definitive method for choosing voxel size based on matching the voxel size to the resolution of the point cloud, which was tested against voxel sizes based on individual tree leaf size, and distance of beam, using destructive samples in Li et al., (2016). Using a radiative transfer approach, the methodology for choosing the "correct" voxel size is not clear, and others' work (and our own additional, unpublished analyses) has shown that estimated PAI values are highly sensitive to voxel size choice.

We have amended our discussion of voxel size in section 1.2 to reflect the contentious debate around voxel size choice, L108-113:

"However, PAI estimates derived using the voxel method are highly dependent on voxel size (Calders et al., 2020). Using a radiative transfer approach, Béland et al., (2014) demonstrated that voxel size is conditional on canopy clumping, radiative transfer model assumptions and occlusion effects, making a single, fixed choice of voxel size within methods for all datasets impossible. To test various approaches to selecting voxel size using a voxel classification approach, Li et al., (2016) matched voxel size to point cloud resolution, individual tree leaf size, and minimum beam distance and tested against destructive samples, finding that voxel size matched to point cloud resolution had the closest PAI values to destructive samples."

To clarify our justification for use of a voxel classification approach over a radiative transfer approach, also commented on by reviewer 1, we have added to section 2.4 (L197-199):

"We chose a voxel classification approach as this method is widely applicable to a range of TLS systems and levels of processing as well as providing explicit guidance on voxel size selection, which is known to impact derived PAI estimates (Li et al., 2016)."

2.10 Optimizing the TLS-based WAI assessment methods, summarizing the regulation of interspecific WAI variation, and using these rules to improve the LAI

assessment will make this article more attractive to better support research in related fields.

We thank the reviewer for their suggestion of including analysis of interspecific WAI variation, which we think is a valuable addition to the paper, and refer to our response to previous comments (2.2, 2.4, 2.11), where we have included these new analyses.

Here, we've focussed on interspecific variation in alpha and PAI, rather than WAI and LAI, but recognise that there would be value in such an additional set of analyses. We agree that developing new methods to correct for WAI in LAI estimates using approaches assessed in this paper would make for exciting work, however we think that to do this well we would require further testing and validation, ideally using destructive samples or multitemporal leaf on/leaf off remote sensing data, which is beyond the scope of this paper.

The following are some detailed points. I hope they will help improve the current edition.

2.11 I suggest authors clarify their research goal in the initial section of the manuscript. As a reader, I am more interested in how to use TLS to analyze WAI. However, authors did not briefly introduce the WAI extraction methods in the abstract but focused on comparing point cloud extraction methods of PAI and LAI.

We apologise for the lack of clarity in explaining our research goals. As in our response to comment 2.1, we have restated our primary and secondary research goals in section 1.3 (L132-133).

We thank the reviewer for their suggestion of analysing WAI, which we think has significantly improved the manuscript. As for comment 2.4, we have now included this analysis. We have chosen to keep the focus on comparing α , as this value is widely discussed in the literature. We have added a statement to this effect (L234-235):

"To allow a comparison with existing literature estimating α , (Sea et al., 2011; Woodgate et al., 2016) we focused on α values."

2.12 They focused on the wood to total plant area (α). I wonder if it is feasible to measure the plant area because of the occlusion effect during scanning. TLS may be more suitable for analyzing WAI.

We apologise not clearly stating the reasons for comparing PAI rather than WAI. All remote sensing methods evaluated in this paper (three TLS methods and DHP) more directly measure PAI than WAI or LAI as sensors are measuring the whole plant. Correcting for wood/ leaf to derive WAI/ LAI requires additional processing steps, which vary according to sensor (wood/ leaf separation algorithms for TLS and image masking for DHP, as these systems are not deciduous, and therefore leaf-off scans can't be made), introducing bias and limiting our ability to compare output. We have added a statement to this effect to section 2.6 (L241-242):

"We chose to compare PAI values rather than WAI or LAI as each method corrects for non-photosynthetic elements in different ways and would introduce bias, limiting the ability to directly compare metrics."

Please see also our response to comment 2.2

We agree that occlusion is a known problem with TLS data in closed canopy forests, however we have minimised the potential occlusion effects by following a dense scanning strategy following the widely cited Wilkes et al., (2017).

2.13 Section 1.3 It will be more interesting to add some research topics on integrating the fine-scale WAI (or α) assessed based on TLS to correct the large-scale LAI extracted from the multi-source remote sensing images. Based on the high-quality field dataset, it should be feasible to use this research in optimizing the large-scale LAI distribution evaluation.

We agree this is an exciting idea and could be the focus of follow-on work. We think that the work presented and, as the reviewer points out, our dataset provides a foundation for a more robust comparison of LAI and new insights from multi-source RS datasets, but that this would be an additional methodological development beyond the scope of our current study.

Following your suggestion, we have added a comment to this effect on L429-430:

"The work presented here provides a foundation for future work combining multi-source and multi-scale remote sensing datasets to correct largescale LAI products."

2.14 In Sections 2.1 and 2.2, the location map of study plots and some images showing the scene of plots should be provided. The pictures of tree species also need to be added to show their phenotypic characteristics, which is beneficial to evaluate their drought tolerance (L323-324).

We agree with the reviewer that a location map of the study plots would be beneficial to the manuscript and thank them for the suggestion. We have therefore added a new figure, B1 to Appendix B showing the locations of plots within the two field sites, Alto Tajo and Cuellar in central Spain.

We believe that the plots used in this study are well studied and documented in the literature and therefore a detailed description of individual plot characteristics would repeat information already available. We have added signposting to this in section 2.1 (L143-144):

"We collected TLS and DHP data from 29 plots in Alto Tajo Natural Park (40°41'N 02°03'W; FunDIV plots; see Baeten et al., (2013) for detailed description of plots)"

The five focus species of this manuscript are widely studied and known species and therefore believe that adding individual images of each species is unnecessary.

2.15 L 191 When setting this threshold (> 0 points) to identify the filled voxels, did you filter noisy points out from the tree TLS datasets? It is not easy to identify and filter all noise in TLS data. I am worried the noise would lead to a lower P_{gap} and cause inaccurate LAI and PAI.

We apologise for not making explicit the noise filtering process of our data. We denoised individual-tree point clouds using height dependant statistical filtering as outlined in Owen et al., (2021), and combined individual tree point clouds into whole plots. We have added a statement to this effect to section 2.4 (L199-200):

"We re-combined individually segmented trees, filtered for noise using a height-dependent statistical filter (see Owen et al., 2021) back into whole plot point clouds"

While any remaining noise may indeed lead to lower P_{gap} , we followed standard processing procedure for this voxel classification method outlined in Hosoi and Omasa, (2006) and tested using destructive samples in Li et al., (2016). Similarly, we followed standard protocol in the published literature for the other two methods (LiDAR Pulse and 2D intensity Image), and therefore consider that our work is a fair representation of each methods' ability to accurately derive PAI and allows a comparison of each methods' merits and drawbacks.

2.16 L203-204 Some structure features of woody and foliage materials can be analyzed based on the pointset-, height bin-, and patch-based models. Please revise this sentence.

We apologise for the lack of clarity in this statement, and thank the reviewer for their suggestion. What we meant to say was that the voxel-based approach was the only method compared in this study capable of analysing PAI, WAI and LAI of segmented individual tree point clouds. We have reworded to make this clear and L215-216 now reads:

"As the only method using multiple co-registered scans, the Voxel-Based method is the only method compared in this study capable of deriving PAI, WAI and LAI of segmented individual tree point clouds."

2.17 L206 The principle of TLS segmentation methods needs to be briefly introduced before the voxelization step. It is beneficial to improve the readability of the manuscript.

We thank the reviewer for their suggestion of providing an explanation of the segmentation process. Trees were not segmented for this paper; we used data that had already been segmented by the authors for a separate study (Owen et al., 2021), and we apologise for the lack of clarity. We have amended the description of tree segmentation in section 2.5 (L218 – 221):

"We used individual tree point clouds downsampled to 0.05 m, to aid computation time, and segmented using the automated tree segmentation program treeseg (Burt et al., 2019), implemented in C++, by Owen et al., (2021) for that study. Individual segmented tree data are available in Owen et al., (2022)."

2.18 L216 How to analyze the WAI after voxelizing woody point clouds? Some details should be introduced, which is key to calculating E' .

We thank the reviewer for their comment and apologise for the lack of clarity in our methods for calculating individual tree WAI. Individual tree WAI was calculated in the same way (voxel classification method) as individual tree PAI, but using the wood-only cloud from the wood – leaf separation step. We have changed L232-233 in section 2.5:

"In the same way as for PAI, we calculated WAI using the separated wood point cloud within the projected crown area of the whole tree (Figure 2d; using the whole crown and not just the wood point cloud)"

2.19 L225 Why explore the relationship between PAI and CAI in this study? The CAI assessment seems to deviate from the research topic, as it is not highly related to LAI and WAI but to the crown projection area, except the canopy gap area. Moreover, using images for CAI analysis is sufficient.

We apologise for not clearly stating our justification for the use of CAI in this study. CAI is used in this study as an indicative measure of both stand density and local competition, and

is included to both explore how PAI is affected by competition, but also to correct for anticipated competitive affects that would otherwise impact our conclusions on species' differences in alpha. We thank the reviewer for their comment, and have amended our manuscript section 2.6 (L245 – 248).

Please see also our response to comment 2.8.

In closed canopies or canopies with crown overlap imagery would not capture CAI, since CAI is calculated using the sum of all projected crown area, not only that visible from imagery. We used TLS to measure CAI as CAI estimates are generated from the sum of all tree crown projected area and so requires individual tree measurements, either from segmented TLS or from ground measurements.

2.20 L245 As shown in Figure 3, PAI estimated using the LiDAR Pulse method more strongly agreed with DHP PAI than the Intensity Image method. However, I found their correlation (R^2) is not particularly significant.

We believe this is a misreading of our meaning, and therefore apologise for not using clear language in reporting our statistical results. We have therefore amended section 3.1 (L266-268):

"Of the two single scan TLS methods tested (LiDAR Pulse method and 2D Intensity Image method), we found that the relationship between PAI estimated using the LiDAR Pulse method and DHP PAI, had a higher R^2 than the 2D Intensity Image method"

2.21 L248 Please carefully recheck the description of the results is correct according to Figure 3. As shown in Figure 3a, the Pulse-based method overestimates the PAI, while the intensity-based method underestimates the PAI.

We apologise for the lack of clarity in explaining these results and meant to say that both methods underestimate relative to DHP at larger values. We have therefore amended the sentence in section 3.1 (L270 -271):

"At larger PAI values, relative to DHP, both TLS methods underestimated PAI compared with DHP (Figure 3b)."

2.22 L264 You did not label Voxel-Based PAI in Figure 3. Do you mean the TLS PAI

We apologise for the lack of clarity in this sentence. Section 3.2, L286 is referring to whole plot plant area index (Figure 4), which does include Voxel-Based PAI. We have now removed the reference to Figure 3 from this sentence.

2.23 L269 Maybe you did not set a suitable threshold when defining blank voxels. Merely my speculation!

We thank the reviewer for their speculation on why we may be experiencing overestimation from Voxel-Based PAI estimates. We followed standard protocol as described in the published literature for the Voxel-Based, LiDAR Pulse and 2D Intensity Images methods, which has allowed us to draw a fair comparison between derived PAI values from each method. Although threshold values could be influencing PAI estimates, we have made a 'best choice' to classify non-zero point containing voxels as vegetation and believe that, while important research, further exploration of threshold values would be beyond the scope of this study.

Please see also response to comment 2.15.

2.24 L282 and 257 You forget to mark the 1:1 dash line in these figures.

This graph (Figure 4b) presents the variation in PAI against CAI in order to understand how competition and stand density affects PAI so we would not assume a 1:1 relationship. Dashed line on Figure 3b is at 0 to highlight systematic variation in the residuals.

We apologise for the lack of clarity and have amended L308 to make this clearer:

“Dashed line in panel a represents 1:1 relationship”

In Figure 3b, the dashed line represents 0, as this panel is showing the relationship between TLS residuals and DHP PAI. We apologise for the lack of clarity and have amended L280:

“Dashed line in panel a represents 1:1 relationship.”

And L281:

“dashed line in panel b represents 0”

2.25 Although authors used the published woody-and-foliage separation methods, it is necessary to display some examples of TLS separation results scanned from diverse plots grown with different species. Due to the lack of validation data, it may be challenging to evaluate the segmentation accuracy. However, presenting the separation results is still available to support visual evaluation.

We agree that showing an example visual assessment of wood/ leaf separation is beneficial to the reader and have included an example of a wood/ leaf separated *P. sylvestris* in Figure 2, panels a and b. We have now included signposting in the figure caption, L212-213:

*“Panels a and b show wood and leaf separation of an example *P. sylvestris*, carried out using TLSeparation (Vicari et al., 2019).”*

We also note that wood – leaf separation was carried out by the authors for a separate published study (Owen et al., 2021). We apologise for the lack of clarity and have changed our description of the wood – leaf separation process accordingly in section 2.5 (L223-225). Please see our response to comment 2.33 below.

2.26 It is not easy to accurately separate the branch and leaf point clouds of trees except those of broadleaf. More importantly, I am worried about whether it is applicable to use the same voxel size to calculate the WAI of different tree species, which is crucial to the conclusion.

Although we agree it may theoretically be more difficult to separate wood and leaf in needleleaf trees, we note that TLSeparation was developed with applicability to both types of trees, with separation difficulties attributable to scanning strategy rather than separation algorithm (Vicari et al., 2019b). We note that this problem was minimised to the best of our ability in our dataset, as we followed a dense scanning strategy as outlined in Wilkes et al., (2017). As for comment 2.25 above, we have included an example visual assessment of a wood – leaf separated (needleleaf) *P. sylvestris* and included signposting in L212-213:

*“Panels a and b show wood and leaf separation of an example *P. sylvestris*, carried out using TL Separation (Vicari et al., 2019).”*

2.27 L294-297 These sentences are not clear. How to assess tree-specific drought tolerance? You would better add some description about its evaluation methods and list the metrics to evaluate the drought tolerance of different tree species in this figure and the related references.

We agree the source of drought tolerance rankings needs to be clear and apologise for omitting this in the figure caption. Drought tolerance are taken from the widely-cited Niinemets and Valladares, (2006). We have amended L326:

“Drought tolerance rankings are taken from Niinemets and Valladares, (2006)”

2.28 In section 4.1, why did you discuss the plot-scale CAI variation? The topic of this section is comparing diverse approaches to deriving PAI.

We apologise for the lack of clarity around the role of CAI in this study. As CAI was used as an indicative measure of stand density and local competition, it was discussed in this section as plots with higher CAI (and therefore greater stem density) showed greater variation in estimated PAI values from each method/ sensor. We note that we have now updated our description of CAI and its role in this study in section 2.6 (L245 – 248) and hope that the discussion in section 4.1 is now more clear.

Please see also our response to comment 2.8.

2.29 The title of Section 4.2 is a phenomenon that you need to analyze. Sections 4.2 and 4.3 still belong to Section 4.1 to discuss the LiDAR-extracted metrics with that of DHP.

The titles of sections 4.2 and 4.3 were intended to emphasise findings of particular interest and relevant to the initial aims of this manuscript. We agree, however, with the reviewer that these sections belong with 4.1 and have removed these section titles to make this more clear.

2.30 L320 According to the field data and Figure 3, what is a very low PAI value? Providing a quantitative indicator will significantly improve the manuscript's readability than using adjective words.

We thank the reviewer for the comment and agree that more quantitative language would improve the manuscript. We have therefore amended L342 to say:

“except at very low PAI values ($PAI_{TLS} < 0.5$).”

2.31 L348 The highest R^2 does not show a strong correlation.

We thank the reviewer for their comment and agree that we have not used clear statistical language. We have therefore changed the wording in L377 – 378:

“The relationship between the LiDAR Pulse method and TLS derived CAI had the highest R^2 ”

2.32 L374 This sentence is not clear. “Although species explain some variation in α , tree height and plot CAI were stronger predictors for all species....” According to the principle of these parameters, it is hard for me to agree that CAI and WAI have a strong correlation.

We agree with the reviewer that we have not used clear statistical language. We have therefore changed this sentence in section 4.5 (L403):

“Although species had a weak relationship with α , tree height and plot CAI had a statistically significant relationship with α ($p<0.001 - p<0.05$) for all species, showing the importance of local stand structure on leaf and woody allocation.”

2.33 L390-392 This is an interesting point. I prefer you to provide some figures and statistical information to prove your finding, especially in different plots with variable growing patterns (growing density, CAI, and WAI related to the tree species, as you mentioned in the Conclusion section). It is beneficial to deepen this study topic.

We thank the reviewer for finding this point interesting and their suggestion of including quantitative results of wood – leaf separation. The discussion point the reviewer refers to is a reference to the published paper describing the wood – leaf separation algorithm. Due to the lack of validation data, evaluating quantitatively the effectiveness of the wood – leaf separation algorithm over the different tree sizes/ growing conditions is not possible for this study.

We note that the wood leaf separation process was carried out by the authors, for a separate study (Owen et al., 2021), in which the results are discussed in more detail and segmented tree files made available online, cited as Owen et al., (2022). We apologise for the lack of clarity here and have reworded our description of the wood – leaf separation process in section 2.5 (L223-229):

“To estimate PAI, WAI and α for each tree, we used individual tree point clouds wood – leaf separated by Owen et al., (2021) using the open source Python library TLSeparation (Vicari et al., 2019a), and then used the separated wood point clouds to calculate WAI.

TLSeparation assigns points as either leaf or wood, iteratively looking at a predetermined number of nearest neighbours (knn). The knn of each iteration is directly dependent on point cloud density, since high density point clouds will require higher a knn (Vicari et al., 2019a). The utility package in TLSeparation was used to automatically detect the optimum knn for each tree point cloud.”

2.34 L 398 I agree that correcting WAI can improve the LAI assessment. The TLS-extracted data can support calibrating LAI based on WAI and PAI. The WAI may be similar among single trees of the same tree species. According to your results, the WAI shows a more evident relationship to tree height and stand density. I think the assessed WAI and plot-level PAI can be used to correct regional LAI for the plot or large-scale forests that were growing with limited tree species.

We agree with the reviewer that interspecific WAI values will be of interest to some readers and thank the reviewer for their suggestion, which we think has significantly improved our manuscript. We have included these additional analyses in Appendix C as also discussed in response to comments 2.4 and 2.10. We hope this work sparks further research on improving LAI estimates at large scale.

Some text errors that needed to be corrected are listed as follows:

Thank you for pointing out these errors.

- **Do not use an abbreviation in the title of your manuscript, as many readers in other fields do not know the meaning of TLS.**

We agree with the reviewer that abbreviations should not be used in titles and have amended our title accordingly.

- **I suggest authors unify the reference format throughout their manuscript. Different citation formats appear in the same paragraph may confuse readers.**

We thank the reviewer for their comment and have checked and corrected referencing throughout.

- **L135 What are FunDIV plots?**

Added "Functional Diversity"

- **L142 I do not understand "altitudinal gradient 840 – 1400 m.a.s.l.".**

Changed to "altitudinal range"

- **L167 compare –i%ž compared**

Changed to "compared"

- **L169 and 180 Please note the font size of the subscript in the Pgap. This abbreviation can also be used in line 162.**

Changed to subscript and moved abbreviation to first use.

- **L176 Please add a comma to this sentence.**

Comma added

- **L199 Where are the solid black voxels in Figure 2?**

Changed to "Coloured voxels (green represents leaf and brown represents wood) are filled voxels and grey lines are empty voxels."

- **L209 wood only point clouds?**

Change to “separated wood cloud”

- **L210 TLSeparation classifies points as leaf or wood? This sentence is not clear.**

Changed to “TLSeparation assigns points as either leaf or wood”

- **L219 TLS PAI and DHP PAI? (Using PAI_{TLS} and PAI_{DHP} instead)**

Changed throughout.

- **L234 Please add a comma to this sentence.**

Comma added.

- **L246-248, L264-265 You can mark these metrics in the insets of Figure 3.**

We think it is important to refer to statistical results in the main text of the manuscript for emphasis, however have included them in the figure captions as well for completeness.

- **Points in Figure 3 can be denoted as different marks or colors, such as circles or crosses, red or blue, to make this chart clearer (like the style of Figure 4).**

Changed to circles and triangles.

- **L262 Please unify the term throughout the manuscript. I think TLS whole plot PAI means TLS PAI(PAI_{TLS}).**

Changed to “whole plot PAI_{TLS}”

- **L274-276 You would better mark these metrics in the subfigures of Figure 4.**

We think it is important to refer to statistical results in the main text of the manuscript, however have included them in the figure captions as well for completeness.

- **In Figures 3 and 4, please delete the unit of PAI. The PAI, LAI and WAI are all ratio-type parameters (no need to denote unit).**

Removed units and changed axis labels to new subscript (PAI_{TLS} / PAI_{DHP})

- **L318 TLS – DHP comparisons?**

Changed to “studies comparing PAI_{TLS} with PAI_{DHP}”

- **In this article, authors used lots of open-source software to support their analysis. I suggest they list all applicable packages and download links to make readers easy to use these tools.**

We thank the reviewer for their suggestion of providing a summary of all open-source software used for this manuscript. We have cited all the software used in text and in the reference list at the end of the manuscript. We believe that citing packages in the main body, readers are able to get a more detailed and contextualised explanation of the use in individual software packages.

- Please carefully check the format of all references according to the manuscript preparation guidelines and the latest published papers in Biogeosciences. The current reference format needs to be optimized.

We thank the reviewer for their comment and have checked the reference format.

References

Baeten, L., Verheyen, K., Wirth, C., Bruelheide, H., Bussotti, F., Finér, L., Jaroszewicz, B., Selvi, F., Valladares, F., Allan, E., Ampoorter, E., Auge, H., Avăcăriei, D., Barbaro, L., Bărnăoiaea, I., Bastias, C. C., Bauhus, J., Beinhoff, C., Benavides, R., Benneter, A., Berger, S., Berthold, F., Boberg, J., Bonal, D., Brüggemann, W., Carnol, M., Castagnéyrol, B., Charbonnier, Y., Chečko, E., Coomes, D., Coppi, A., Dalmaris, E., Dănilă, G., Dawud, S. M., de Vries, W., De Wandeler, H., Deconchat, M., Domisch, T., Duduman, G., Fischer, M., Fotelli, M., Gessler, A., Gimeno, T. E., Granier, A., Grossiord, C., Guyot, V., Hantsch, L., Hättenschwiler, S., Hector, A., Hermy, M., Holland, V., Jactel, H., Joly, F.-X., Jucker, T., Kolb, S., Koricheva, J., Lexer, M. J., Liebergesell, M., Milligan, H., Müller, S., Muys, B., Nguyen, D., Nichiforel, L., Pollastrini, M., Proulx, R., Rabasa, S., Radoglou, K., Ratcliffe, S., Raulund-Rasmussen, K., Seiferling, I., Stenlid, J., Vesterdal, L., von Wilpert, K., Zavala, M. A., Zielinski, D., and Scherer-Lorenzen, M.: A novel comparative research platform designed to determine the functional significance of tree species diversity in European forests, *Persepct. Plant. Ecol.*, 15, 281–291, <https://doi.org/10.1016/j.ppees.2013.07.002>, 2013.

Caspersen, J. P., Vanderwel, M. C., Cole, W. G., and Purves, D. W.: How Stand Productivity Results from Size- and Competition-Dependent Growth and Mortality, *PLoS ONE*, 6, e28660, <https://doi.org/10.1371/journal.pone.0028660>, 2011.

Coomes, D. A., Holdaway, R. J., Kobe, R. K., Lines, E. R., and Allen, R. B.: A general integrative framework for modelling woody biomass production and carbon sequestration rates in forests, *Journal of Ecology*, 100, 42–64, <https://doi.org/10.1111/j.1365-2745.2011.01920.x>, 2012.

Hosoi, F. and Omasa, K.: Voxel-Based 3-D Modeling of Individual Trees for Estimating Leaf Area Density Using High-Resolution Portable Scanning Lidar, *IEEE T. Geosci. Remote*, 44, 3610–3618, <https://doi.org/10.1109/TGRS.2006.881743>, 2006.

Kamoske, A. G., Dahlin, K. M., Stark, S. C., and Serbin, S. P.: Leaf area density from airborne LiDAR: Comparing sensors and resolutions in a temperate broadleaf forest ecosystem, *Forest Ecol. Manag.*, 433, 364–375, <https://doi.org/10.1016/j.foreco.2018.11.017>, 2019.

Li, Y., Guo, Q., Tao, S., Zheng, G., Zhao, K., Xue, B., and Su, Y.: Derivation, Validation, and Sensitivity Analysis of Terrestrial Laser Scanning-Based Leaf Area Index, *Can. J. Remote Sens.*, 42, 719–729, <https://doi.org/10.1080/07038992.2016.1220829>, 2016.

Owen, H. J. F., Flynn, W. R. M., and Lines, E. R.: Competitive drivers of inter-specific deviations of crown morphology from theoretical predictions measured with Terrestrial Laser Scanning, *J. Ecol.*, 109, 2612–2628, <https://doi.org/10.1111/1365-2745.13670>, 2021.

Vicari, M. B., Disney, M., Wilkes, P., Burt, A., Calders, K., and Woodgate, W.: Leaf and wood classification framework for terrestrial LiDAR point clouds, *Methods Ecol. Evol.*, 10, 680–694, <https://doi.org/10.1111/2041-210X.13144>, 2019a.

Vicari, M. B., Pisek, J., and Disney, M.: New estimates of leaf angle distribution from terrestrial LiDAR: Comparison with measured and modelled estimates from nine broadleaf tree species, *Agricultural and Forest Meteorology*, 264, 322–333, <https://doi.org/10.1016/j.agrformet.2018.10.021>, 2019b.

Wilkes, P., Lau, A., Disney, M., Calders, K., Burt, A., Gonzalez de Tanago, J., Bartholomeus, H., Brede, B., and Herold, M.: Data acquisition considerations for Terrestrial Laser Scanning of forest plots, *Remote Sens. Environ.*, 196, 140–153, <https://doi.org/10.1016/j.rse.2017.04.030>, 2017.

1 **Quantifying vegetation indices using Terrestrial Laser**
2 **Scanning: methodological complexities and ecological insights**
3 **from a Mediterranean forest**

4 William Rupert Moore Flynn¹, Harry Jon Foord Owen², Stuart William David Grieve^{1,3} and
5 Emily Rebecca Lines²

6 ¹School of Geography, Queen Mary University of London, Mile End Rd, Bethnal Green, London E1 4NS

7 ²Department of Geography, University of Cambridge, Downing Place, Cambridge, CB2 3EN

8 ³Digital Environment Research Institute, Queen Mary University of London, New Road, London, E1 1HH

9 Correspondence to: W. R. M. Flynn (w.r.m.flynn@qmul.ac.uk)

10 **Abstract.** Accurate measurement of vegetation density metrics including plant, wood and leaf area indices (PAI,
11 WAI and LAI) is key to monitoring and modelling carbon storage and uptake in forests. Traditional passive sensor
12 approaches, such as Digital Hemispherical Photography (DHP), cannot separate leaf and wood material, nor
13 individual trees, and require many assumptions in processing. Terrestrial Laser Scanning (TLS) data offer new
14 opportunities to improve understanding of tree and canopy structure. Multiple methods have been developed to
15 derive PAI and LAI from TLS data, but there is little consensus on the best approach, nor are methods
16 benchmarked as standard.

17 Using TLS data collected in 33 plots containing 2472 trees of five species in Mediterranean forests, we compare
18 three TLS methods (*LiDAR Pulse*, *2D Intensity Image* and *Voxel-Based*) to derive PAI and compare with co-
19 located DHP. We then separate leaf and wood in individual tree point clouds to calculate wood to total plant area
20 (α), a metric to correct for non-photosynthetic material in LAI estimates. We use individual tree TLS point clouds
21 to estimate how α varies with species, tree height and stand density.

22 We find the *LiDAR Pulse* method agrees most closely with DHP, but is limited to single scan data so cannot
23 determine individual tree α . The *Voxel-Based* method shows promise for ecological studies as it can be applied to
24 individual tree point clouds. Using the *Voxel-Based* method, we show that species explain some variation in α ,
25 however, height and density were ~~stronger~~ better predictors.

26 Our findings highlight the value of TLS data to improve fundamental understanding of tree form and function,
27 but also the importance of rigorous testing of TLS data processing methods at a time when new approaches are
28 being rapidly developed. New algorithms need to be compared against traditional methods, and existing
29 algorithms, using common reference data. Whilst promising, our results show that metrics derived from TLS data
30 are not yet reliably calibrated and validated to the extent they are ready to replace traditional approaches for large
31 scale monitoring of PAI and LAI.

32

33 **1 Introduction**

34 Terrestrial Laser Scanning (TLS) generates high-resolution 3D measurements of whole forests and individual
35 trees (Burt et al., 2018; Disney, 2018), leading to the development of completely new monitoring approaches to
36 understand the structure and function of ecosystems (Lines et al., 2022). Unlike traditional passive sensors, TLS
37 can estimate plant, wood and leaf area indices (PAI; WAI; LAI) for both whole plots and individual tree point
38 clouds (Calders et al., 2018), and is unaffected by illumination conditions. This has led to the development of
39 several methods for processing TLS data to extract the key metrics PAI, WAI and LAI (e.g. Hosoi and Omasa,
40 2006; Jupp et al., 2008; Zheng et al., 2013). However, intercomparison of algorithms and processing approaches
41 to derive the same metrics from different TLS methods are lacking.

42 Leaf Area Index (LAI), defined as half the amount of green leaf area per unit ground area (Chen and Black, 1992),
43 determines global evapotranspiration, phenological patterns and canopy photosynthesis, and is therefore an
44 essential climate variable (ECV), as well as a key input in dynamic global vegetation models (Sea et al., 2011;
45 Weiss et al., 2004). Accurate measurements of LAI, WAI and PAI have historically been derived from labour
46 intensive destructive sampling (Baret et al., 2013; Jonckheere et al., 2004), so over large spatial or temporal scales
47 these can only be measured indirectly, typically with remote sensing. Large-scale remote sensing, using
48 spaceborne and airborne instruments, has been widely used to estimate LAI over large areas (Pfeifer et al., 2012),
49 but requires calibration and validation using in situ measurements to constrain information retrieval (Calders et
50 al., 2018). Non-destructive in situ vegetation index estimates have historically been made by measuring light
51 transmission below the canopy and using simplifying assumptions about canopy structure to estimate the amount
52 of intercepting material (e.g. Beer-Lambert law; Monsi and Saeki, 1953). The most common method, Digital
53 Hemispherical photography (DHP; Figure 1a), requires both model assumptions and subjective user choices during
54 data acquisition and processing in order to estimate both PAI and LAI (Breda, 2003). DHP images are processed
55 by separating sky from canopy, but not photosynthetic from non-photosynthetic vegetative material, so additional
56 assumptions are needed to calculate either LAI or WAI (Jonckheere et al., 2004; Pfeifer et al., 2012). Separation
57 of LAI from PAI can be achieved by removing or masking branches and stems from hemispherical images (e.g.
58 Sea et al., 2011; Woodgate et al., 2016), but is not reliable when leaves are occluded by woody components
59 (Hardwick et al., 2015). An alternative approach is to take separate DHP measurements in both leaf on and leaf
60 off conditions, and derive empirical wood to plant ratios (WAI/PAI, α) (Leblanc and Chen, 2001), but this is not
61 always practical, for example in evergreen forests. The difficulty of separation means that studies often omit
62 correcting for the effect of WAI on optical PAI measurements altogether (Woodgate et al., 2016), but since woody
63 components in the forest canopy can account for more than 30% of PAI (Ma et al., 2016) this can introduce
64 overestimation. Further, although DHP estimates of LAI or PAI are valuable both for ecosystem monitoring and
65 developing satellite LAI products (Hardwick et al., 2015; Pfeifer et al., 2012), they are limited to sampling only
66 at a neighbourhood or plot level (Weiss et al., 2004), and cannot be used to measure individual tree LAI except
67 for open grown trees (Béland et al., 2014).

68 The ratio of wood to total plant area, α , is known to be dynamic, changing in response to abiotic and biotic
69 conditions. For example, the Huber value (sapwood to leaf area ratio, a related measure to α) may vary according
70 to water availability (Carter and White 2009). Leaf area may therefore be indicative of the drought tolerance level
71 of a tree, with more drought tolerant species displaying a lower leaf area, reducing the hydraulic conductance of

72 the whole tree and therefore increasing its drought tolerance (Niinemets and Valladares, 2006). α has been
73 hypothesised to increase with the size of a tree in response to the increased hydraulic demand associated with
74 greater hydraulic resistance of tall trees (Magnani et al., 2000) and higher transpiration rates of larger LAI
75 (Battaglia et al., 1998; Phillips et al., 2003). Stand density may also impact α (Long and Smith, 1988; Whitehead,
76 1978), as increased stand level water use scales linearly with LAI (Battaglia et al., 1998; Specht and Specht, 1989),
77 reducing water availability to individual trees competing for the same resources (Jump et al., 2017). Large scale
78 quantification of α or Huber value, however, is difficult as studies usually rely on a small number of destructively
79 sampled trees (e.g. Carter and White, 2009; Magnani et al., 2000), litterfall traps (e.g. Phillips et al., 2003) or
80 masking hemispherical images (e.g. Sea et al., 2011; Woodgate et al., 2016). These approaches are only applicable
81 on a small to medium scale, and in the case of image masking, cannot differentiate between individuals. Variation
82 in α , for example by species and or stand structure, is therefore largely unknown.

83 1.2 TLS methods for calculating PAI, LAI and WAI

84 TLS methods for extracting PAI, LAI and WAI can be broadly categorised into two types: (1) LiDAR return
85 counting, using single scan data (e.g., the *LiDAR Pulse* method; Jupp et al., 2008, and *2D Intensity Image* method;
86 Zheng et al., 2013) and (2) point cloud voxelisation, usually using co-registered scans (e.g., the *Voxel-Based*
87 method; Hosoi and Omasa, 2006).

88 The *LiDAR Pulse* method (Jupp et al., 2008; Figure 1b) estimates gap fraction ($P_{gap}P_{gap}$) using single scan data,
89 as a function of the total number of outgoing LiDAR pulses from the sensor and the number of pulses that are
90 intercepted by the canopy. This method, which eliminates illumination impacts associated with the use of DHP
91 (Calders et al., 2014), has been implemented in the python module, *PyLidar* (www.pylidar.org) and the R package,
92 *rTLS* (Guzman, et al. 2021). Using the *LiDAR Pulse* method, Calders et al. (2018) compared [TLS-PAI-PAI](#)
93 estimates from two ground-based passive sensors (LiCOR LAI-2000 and DHP) with TLS data collected with a
94 RIEGL VZ-400 TLS in a deciduous woodland, and found the two passive sensors underestimated PAI values
95 compared to TLS, with differences dependent on DHP processing and leaf on/off conditions.

96 The *2D Intensity Image* method (Zheng et al., 2013; Figure 1c), also uses raw single scan TLS point clouds, but
97 unlike the *LiDAR Pulse* method, this approach converts LiDAR returns into 2D panoramas where pixel values
98 represent intensity. PAI is estimated by classifying pixels as sky or vegetation, based on their intensity value, to
99 estimate $P_{gap}P_{gap}$, and then applying Beer-Lambert's law. As for the *LiDAR Pulse* method, this approach has
100 been shown to generate higher PAI estimates than DHP (Calders et al., 2018; Woodgate et al., 2015; Grotti et al.,
101 2020), with differences attributed to the greater pixel resolution and viewing distance of TLS resolving more small
102 canopy details (Grotti et al., 2020).

103 The *Voxel-Based* method (Figure 1d) estimates PAI by segmenting a point cloud into voxels and either simulating
104 radiative transfer within each cube (Béland et al., 2014; Kamoske et al., 2019), or classifying voxels as either
105 containing vegetation or not, and dividing vegetation voxels by the total number of voxels (Hosoi and Omasa,
106 2006; Itakura and Hosoi, 2019; Li et al., 2017). Crucially, this method may be applied to multiple co-registered
107 scan point clouds and so can be used to calculate PAI for both whole plots and individual, segmented TLS trees.

108 [However, PAI estimates derived using the voxel method are highly dependent on voxel size](#) (Calders et al., 2020).
109 [Using a radiative transfer approach, Béland et al. \(2014\) demonstrated that voxel size is dependent on canopy](#)

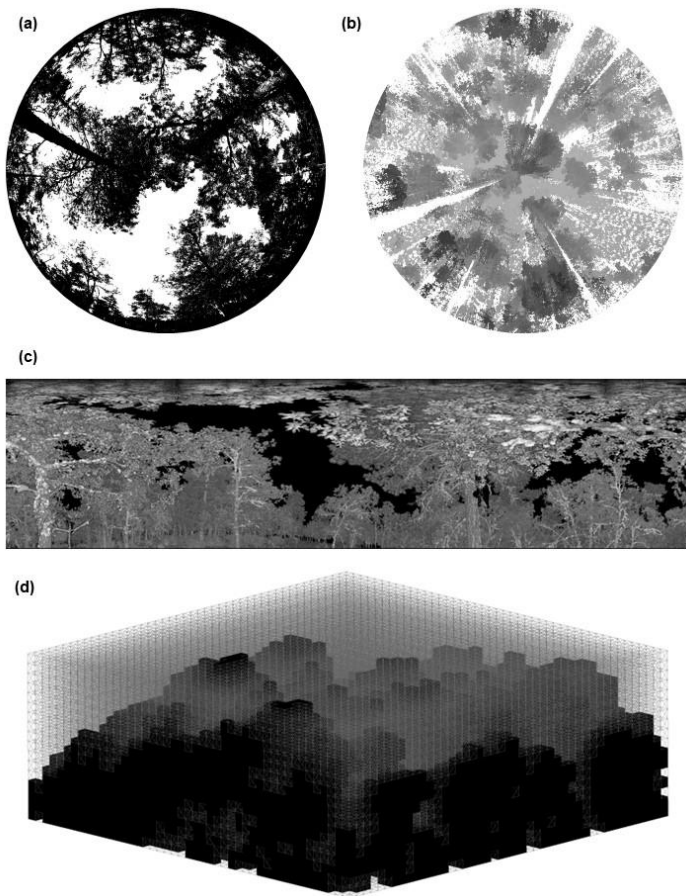
Formatted: Font: 10 pt

Formatted: Font: 10 pt

110 [clumping, radiative transfer model assumptions and occlusion effects, making a single, fixed choice of voxel size](#)
111 [within methods for all datasets impossible. To test various approaches to selecting voxel size using a voxel](#)
112 [classification approach, Li et al., \(2016\) matched voxel size to point cloud resolution, individual tree leaf size,](#)
113 [and minimum beam distance and tested against destructive samples, finding that voxel size matched to point cloud](#)
114 [resolution had the closest PAI values to destructive samples.](#)

115 The *LiDAR Pulse* method and *2D Intensity Image* method both use single scan data. However, to generate robust
116 estimates of canopy properties that avoid errors from occlusion effects, multiple co-registered scans taken from
117 different locations are likely needed (Wilkes et al., 2017). Further, both these methods require raw unfiltered data
118 to accurately measure the ratio of pulses emitted from the scanner and number of pulses that are intercepted by
119 vegetation. This means “noisy” points caused by backscattered pulses (Wilkes et al., 2017) are included in
120 analyses, potentially leading to higher PAI estimates. However, the *LiDAR Pulse* and *2D Intensity Image* methods
121 may introduce fewer estimation errors compared DHP, which is influenced by differences in sky illumination
122 conditions and camera exposure (Weiss et al., 2004).

Formatted: Font: Not Italic



123

124

125 **Figure 1: Methods for PAI estimation applied in this study: (a) a binarised digital hemispherical photograph (DHP),**
126 **(b) TLS raw single scan point cloud, used within the LiDAR Pulse method (Jupp et al., 2008). Image shows a top-down**
127 **view of raw point cloud and greyscale represents low (grey) and high (black) Z values, (c) TLS 2D intensity image for**
128 **the 2D Intensity Image method (Zheng et al., 2013), (d) Voxelsised co-registered whole plot point cloud for the Voxel-**
129 **Based method (Hosoi and Omasa, 2006), showing a representative schematic of cube voxels with edge length of 1m,**
130 **voxelsised using the R package VoxR (Lecigne et al., 2018). Solid black voxels are classified as containing vegetation**
131 **(filled) and voxels outlined with grey lines are voxels classified as empty.**

Formatted: Font: Not Bold

132 1.3 Scope and aims

133 The aims of this study are twofold: the first aim is to compare three TLS methods for estimating PAI with
134 traditional DHP. The second aim of this study is to use TLS to drivers of individual tree α variation.

Formatted: Font: Not Bold

135 In this study we use a dataset of 528 co-located DHP and high-resolution TLS scans from 33 forest plots to
136 compare DHP derived PAI (PAI_{DHP}) with estimates from three methods to estimate PAI from TLS data (PAI_{TLS}):
137 the *LiDAR Pulse* method; the *2D Intensity Image* method and the *Voxel-Based* method (Figure 1). We use a dataset
138 collected from a network of pine/oak forest plots in Spain (Owen et al., 2021) and ask (1) are the three TLS
139 methods able to reproduce $DHP-PAI_{DHP}$ estimates at single scan and whole plot level? (2) does α , calculated
140 from the *Voxel-Based* method on individual tree point clouds, vary with species and tolerance to drought; and (3)
141 does α scale with height and stand density?

Formatted: Subscript

142 2. Methods

143 2.1 Study site

144 We collected TLS and DHP data from 29 plots in Alto Tajo Natural Park ([40°41'N 02°03'W](#); FunDIV ([Functional](#)
145 [Diversity](#)) plots; [see Baeten et al., \(2013\) for detailed description of plots](#)) and four plots in Cuellar
146 ([41°23'N 4°21'W](#)) in June - July 2018 (see Owen et al., [\(2021\) for full details](#)) ([Figure B1](#)). Plots contained two
147 oak species: semi-deciduous *Q. faginea* and evergreen *Q. ilex*, and three pine species: *P. nigra*, *P. pinaster* and *P.*
148 *sylvestris*. *P. sylvestris* is the least drought tolerant species, followed by *P. nigra*, *Q. faginea*, *Q. ilex*; shade
149 tolerance follows the same ranking (Niinemets and Valladares, 2006; Owen et al., 2021). Although not
150 quantitatively ranked, *P. pinaster* has been shown to be very drought tolerant, appearing in drier areas than the
151 other species (Madrigal-González et al., 2017). The area is characterised by a Mediterranean climate (altitudinal
152 [gradient range](#) 840 – 1400 m.a.s.l.) (Jucker et al., 2014; Madrigal-González et al., 2017). In addition to the five
153 main canopy tree species, plots contained an understory of *Juniperus thurifera* and *Buxus sempervirens* (Kuusk
154 et al., 2018).

155 2.2 Field protocol

156 In each of the 33 30 x 30 m plots we collected TLS scans on a 10 m grid, making 16 scan locations following
157 Wilkes et al., (2017) to minimise occlusion effects associated with insufficient scans. We used a Leica HDS6200
158 TLS set to super high resolution (3.1 x 3.1mm resolution at 10 m with a beam divergence of ≤ 5 mm at 50 m; scan
159 time 6m 44 s; [see Owen et al., \(2021\)](#)). At each of the 528 scan locations and following the protocol in Pfeifer et
160 al., (2012), we captured co-located DHP images with three exposure settings (automatic and \pm one stop exposure
161 compensation), levelling a Canon EOS 6D full frame DSLR sensor with a Sigma EX DG F3.5 fisheye lens,
162 mounted on a Vanguard Alta Pro 263AT tripod.

163 **2.3 Calculation of single scan and whole plot PAI using DHP data**

164 For each of the red-green-blue (RGB) DHP images we extracted the blue band for image thresholding, as this best
165 represents sky/vegetation contrast (Pfeifer et al., 2012). For each plot, we picked the exposure setting that best
166 represented sky/ vegetation difference based on pixel brightness histograms of four sample locations indicative of
167 the plot. We carried out automatic image thresholding using the Ridler and Calvard method (1978), to create a
168 binary image of sky and vegetation, avoiding subjective user pixel classification (Jonckheere et al., 2005). We
169 calculated PAI from the binary image, limiting the field of view to a 5° band centred on the hinge angle of 57.5°
170 (55° – 60°). The hinge angle has a path length through the canopy twice the canopy height, so the band around it
171 is an area of significant spatial averaging taken as representative of canopy structure of the area (Calders et al.,
172 2018; Jupp et al., 2008). From the binarised hinge angle band we calculated P_{gap} as the number of sky
173 pixels divided by the total number of pixels and PAI using an inverse Beer-Lambert law equation (Monsi and
174 Saeki, 1953). We calculated whole plot PAI as the arithmetic mean within plot scan location PAI. As this value
175 does not correct for canopy clumping, it is better described as effective PAI, rather than true PAI (Woodgate et
176 al., 2015). However, as the TLS and DHP methods we apply here account for canopy clumping differently, we
177 compared effective values and here-on refer to effective PAI as PAI (Calders et al., 2018).

178 **2.4 Calculation of single scan and whole plot PAI from TLS data**

179 To calculate PAI using the *LiDAR Pulse* method (Jupp et al., 2008), we calculated the P_{gap} for a
180 single scan (Figure 1b) by summing all returned laser pulses and dividing by the number of total outgoing pulses,
181 following Lovell et al. (2011; see Eq. 7 in that study), and then estimated PAI following Jupp et al. (2008; see Eq.
182 18 in that study), setting the sensor range to 5° around the hinge angle as before (55° – 60°). Single scan PAI was
183 taken as the cumulative sum of PAI values estimated by vertically dividing the hinge region into 25 cm intervals
184 (Calders et al., 2014). We implemented the *LiDAR Pulse* method using the open-source *R* (R Core Team, 2020)
185 package, *rTLS* (Guzmán and Hernandez, 2021).

Formatted: Subscript

186 To calculate PAI using the *2D Intensity Image* method (Zheng et al., 2013), we converted 3D TLS point cloud
187 data from all 528 scan locations into polar coordinates and scaled intensity values to cover the full 0–255 range
188 (Figure 1c) and rasterised into a 2D intensity image using the open-source *R* package, *raster* (Hijmans, 2022). We
189 cut the 2D intensity image to a 5° band around the hinge angle (55° – 60°) and classified sky and vegetation pixels
190 in each image using the Ridler and Calvard method (1978). We calculated P_{gap} as the number of pixels classified
191 as sky divided by the total number of pixels and derived PAI with an inverse Beer-Lambert law equation (Monsi
192 and Saeki, 1953).

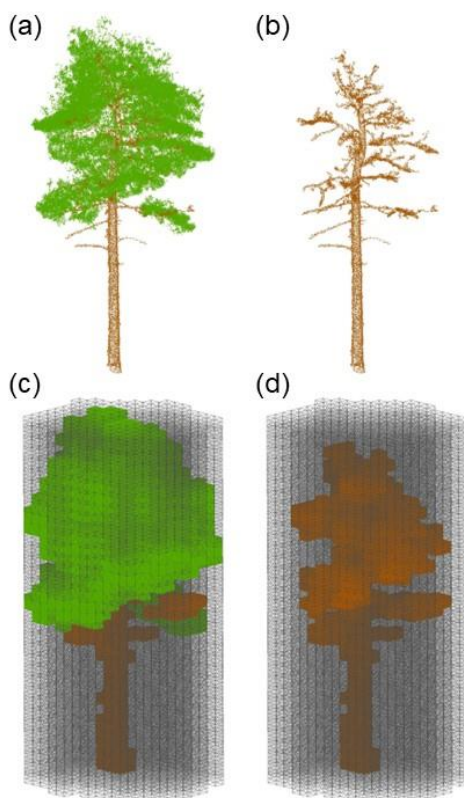
Formatted: Subscript

193 Following the same approach as applied to our DHP data, we calculated whole plot PAI for the *LiDAR Pulse* and
194 *2D Intensity Image* methods as the arithmetic mean of within plot single scan PAI estimates.

195 To calculate PAI using the *Voxel-Based* method, we followed a voxel classification approach (Hosoi and Omasa,
196 2006), *downsampling the point cloud to 0.05 m to aid computation time and* matching the voxel size to the
197 resolution of the point cloud (0.05 m), following Li et al., (2016), who showed that matching the voxel size to
198 the point cloud point to point minimum distance (resolution) increases accuracy as small canopy gaps are not
199 included in voxels classified as vegetation. *We chose a voxel classification approach as this method is widely*
200 *applicable to a range of TLS systems and levels of processing as well as providing explicit guidance on voxel size*

201 [selection, which is known to impact derived PAI estimates](#) (Li et al., 2016). We re-combined individually
 202 segmented trees, [filtered for noise using a height-dependent statistical filter](#) (see Owen et al., 2021) [back](#) into
 203 whole plot point clouds and voxelised them using the open source *R* package, *VoxR* (Lecigne et al., 2018), with a
 204 full grid covering the minimum to maximum XYZ ranges of the plot. We classified any voxel containing > 0
 205 points as vegetation (“filled”), and empty voxels as gaps. We then split the voxelised point cloud into slices one
 206 voxel high. Within each slice, the contact frequency is calculated as the fraction of filled to total number of voxels.
 207 We then multiplied the contact frequency by a correction factor for leaf inclination, set at 1.1 (Li et al., 2017), and
 208 whole plot PAI was calculated as the sum of all slices’ contact frequencies.

209 **2.5 Calculation of individual tree PAI, WAI and α using the voxel-based method**



210 **Figure 2:** Visualisation of the workflow for applying the Voxel-Based method to estimate individual-tree PAI, WAI and
 211 α . (a) Individual tree point cloud; (b) separated leaf off (wood) individual tree point cloud; (c) voxelised individual tree
 212 point cloud; (d) voxelised wood cloud. [Solid black-Coloured voxels \(green represents leaf and brown represents wood\)](#)
 213 are filled voxels and grey lines are empty voxels. Empty voxels occupy the space within the projected crown area of the
 214 tree. Image shows schematic of point cloud voxelised with cube voxels with edge length of 0.5 m. [Panels a and b show](#)
 215 [Wwood and leaf separation of an example *P. sylvestris*, was](#) carried out using *TLSeparation* (Vicari et al., 2019). Point
 216 cloud voxelisation was carried out using modified functions from *R* package *VoxR* (Lecigne et al., 2018).

217 As the only method using multiple co-registered scans, the *Voxel-Based* method is only method [compared in this](#)
218 [study we found](#) capable of [deriving PAI, WAI and LAI of segmented individual tree point clouds estimating](#)
219 [individual tree leaf and wood properties](#). We estimated PAI and WAI for 2472 individual trees segmented from
220 co-registered point clouds following a similar method to the whole plot point cloud. We [used individual tree point](#)
221 [clouds downsampled to 0.05 m, to aid computation time, and extracted segmented individual trees](#) using the
222 automated tree segmentation program *treeseg* (Burt et al., 2019), implemented in C++, [see by](#) Owen et al., (2021)
223 for [that study, full details, and Individual segmented tree data are available in](#) Owen et al., (2022) [for individual](#)
224 [segmented tree data](#).

225 To estimate PAI, WAI and α for each tree, we [first separated leaf from wood points in used](#) individual tree point
226 [clouds wood – leaf separated by](#) (Owen et al., (2021) using the open source Python library *TLSeparation* (Vicari
227 et al., 2019), and then used the [separated](#) wood [only](#) point clouds to calculate WAI. *TLSeparation* [classifies](#)
228 [assigns](#) points [as as either](#) leaf or wood, iteratively looking at a predetermined number of nearest neighbours (knn).
229 The knn of each iteration is directly dependent on point cloud density, since high density point clouds will require
230 higher a knn (Vicari et al., 2019). [We used t](#)The utility package in *TLSeparation* [was used](#) to automatically detect
231 the optimum knn for each tree point cloud.

232 To voxelize individual tree complete (Figure 2a) and wood only (Figure 2b) point clouds, we used a modified
233 approach based on Lecigne et al., (2018), voxelising within the projected crown area of the whole tree point cloud
234 (Figure 2c) to calculate PAI. [In the same way as for PAI, wWe](#) calculated WAI [using the separated wood point](#)
235 [cloud](#) within the projected crown area of the whole tree (Figure 2d; using the whole crown and not just the wood
236 point cloud), and derived α for each tree as WAI/PAI . [To allow a comparison with existing literature estimating](#)
237 [a, \(Sea et al., 2011; Woodgate et al., 2016\) we focused on a values.](#)

238 2.6 Statistical Analyses

239 We tested the relationships between [TLS-PAI](#) PAI_{TLS} and [DHP-PAI](#) PAI_{DHP} estimates using Standardised Major
240 Axis (SMA) using the open source *R* (R Core Team, 2020) package, *smatr* (Warton et al., 2012). SMA is an
241 approach to estimating a line of best fit where we are not able to predict one variable from another (Warton et al.,
242 2006); we chose SMA because we do not have a ‘true’ validation dataset, so avoid assuming either DHP or any
243 of the TLS methods produces the most accurate results. For each TLS method, we assessed the relationship with
244 DHP using the coefficient of determination and RMSE. [We chose to compare PAI values rather than WAI or LAI](#)
245 [as each method corrects for non-photosynthetic elements in different ways and would introduce bias, limiting the](#)
246 [ability to directly compare metrics](#). To further understand observed drivers of variance in PAI, we tested the
247 relationship between PAI and TLS estimated whole plot crown area index, CAI, calculated as the sum of projected
248 crown area, divided by the plot area (Owen et al., 2021), [and indicative and a proxy](#) measure of stand density [and](#)
249 [local competition](#) (Caspersen et al., 2011; Coomes et al., 2012), using SMA.

250 To test if α differs by species, we used linear mixed models (LMMs) in the *R* package, *lme4* (Bates et al., 2015).
251 We included an intercept only random plot effect to account for local effects on α :

252

$$253 \alpha_{i,sj} = \alpha_s + Plot_j \quad (1)$$

Formatted: Subscript

Formatted: Subscript

254

255 here, α_i is α of an individual of species s , in plot j , and a_s is the parameter to be fit. To test the effect of stand
256 structure and tree height on α_i , we fit relationships separately for each species, again including a random plot
257 effect:

258

259
$$\alpha_{i,sj} = a_s + b_s H_i + c_s CAI_j + Plot_{sj} \quad (2)$$

260

261 here H_i is the height of the tree, CAI_j is the crown area index for the plot, with other parameters as before.

262 For each species' model (equation 2), we calculated the intra-class correlation coefficient (ICC). The ICC, similar
263 to coefficient of determination, quantifies the amount of variance explained by the random effect in a linear mixed
264 model (Nakagawa et al., 2017).

265 **3. Results**

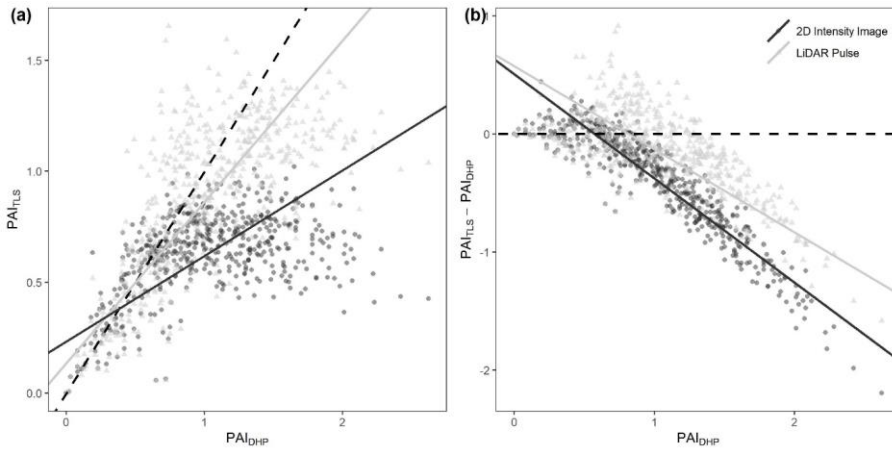
266 **3.1 Comparison of plant area index estimated by DHP and single scan TLS**

267 Of the two single scan TLS methods tested (*LiDAR Pulse* method and *2D Intensity Image* method), we found that
268 the relationship between PAI estimated using the *LiDAR Pulse* method and more strongly agreed with DHP
269 PAIPAI_{DHP}, but there was also significant correlation for had a higher R² than the *2D Intensity Image* method
270 (SMA; *LiDAR Pulse* method $R^2 = 0.50$, slope = 0.73, $p < 0.001$, RMSE = 0.14, and *2D Intensity Image* method R^2
271 = 0.22, slope = 0.38, $p < 0.001$, RMSE = 0.39, respectively, Figure 3a). At larger PAI values, relative to DHP, both
272 TLS methods underestimated PAI compared with DHP (Figure 3b). We found statistically significant negative
273 correlations between residuals and DHP for both methods (SMA; *2D Intensity Image* method residuals $R^2 = 0.85$,
274 slope = -0.88, $p < 0.01$; *LiDAR Pulse* method residuals $R^2 = 0.47$, slope = -0.70, $p < 0.01$; Figure 3b). The *2D*
275 *Intensity Image* method showed larger underestimation at higher DHP PAIPAI_{DHP} values, suggesting this method
276 may saturate sooner than both DHP and the *LiDAR Pulse* method at higher PAI values (Figure 3b).

Formatted: Subscript

Formatted: Superscript

Formatted: Subscript



277

278 **Figure 3: Comparison of single scan TLS-PAI and DHP-PAI estimates, for all 528 scan locations (16 per**
 279 **plot). (a) The correlation between DHP derived PAI with PAI derived using the 2D Intensity Image method $R^2 = 0.22$,**
 280 **slope = 0.38, $p < 0.001$, RMSE = 0.39 (circles), and LiDAR Pulse method $R^2 = 0.50$, slope = 0.73, $p < 0.001$, RMSE = 0.14**
 281 **(triangles). Dashed line in panel a represents 1:1 relationship, (b) The difference between $\text{TLS-PAI}_{\text{TLS}}$ and $\text{DHP-PAI}_{\text{DHP}}$**
 282 **estimates for the 2D Intensity Image method, and LiDAR Pulse method (dashed line at in panel b represents**
 283 **0). Lines show statistically significant relationships fitted using SMA ($p < 0.01$).**

284 **3.2 Comparison of whole plot plant area index estimated using TLS and DHP and the effect of plot structure**
 285 **on PAI**

286 We found statistically significant correlations between whole plot TLS whole plot PAI_{TLS} values and DHP
 287 PAI_{DHP} for all three TLS methods. As for single scans (Figure 3), the LiDAR Pulse method showed the closest
 288 agreement to DHP PAI_{DHP}, here compared to both the Voxel-Based and 2D Intensity Image methods (SMA;
 289 LiDAR Pulse method $R^2 = 0.66$, slope = 0.82, $p < 0.01$, RMSE = 0.14; Voxel-Based method $R^2 = 0.39$, slope = 2.76,
 290 $p < 0.01$, RMSE = 0.88; 2D Intensity Image method $R^2 = 0.35$, slope = 0.36, $p < 0.01$, RMSE = 0.39, respectively;
 291 Figure 4a). The 2D Intensity Image method and LiDAR Pulse method consistently underestimated PAI compared
 292 to DHP, whilst the Voxel-Based method underestimated in plots with lower DHP PAI_{DHP} and overestimated
 293 in plots with higher DHP PAI_{DHP}. The Voxel-Based method's high PAI values compared to other methods is
 294 likely due to its use of multiple co-registered scans reducing occlusion effects prevalent in single scan data.

295 To assess the effect of plot structure on variation in TLS derived PAI, we compared TLS-PAI estimates to
 296 TLS estimated crown area index (CAI, m^2 projected crown area per m^2 ground area, Figure 4b). We found a
 297 significant positive relationship between CAI and PAI estimated using each of the LiDAR Pulse method, the
 298 Voxel-Based method, and DHP (SMA; LiDAR Pulse method $R^2 = 0.79$, slope = 1.69, $p < 0.01$; Voxel-Based method
 299 $R^2 = 0.76$, slope = 5.72, $p < 0.01$; 2D Intensity Image method $R^2 = 0.15$, slope = 0.76, p < 0.05; DHP $R^2 = 0.46$,
 300 slope = 2.07, $p < 0.01$, respectively; Figure 4b), where the 2D Intensity Image method appears to saturate at medium
 301 CAI values (Figure 4b).

Formatted: Subscript

Formatted: Subscript

Formatted: Font: 9 pt, Bold

Formatted: Font: 9 pt, Bold

Formatted: Subscript

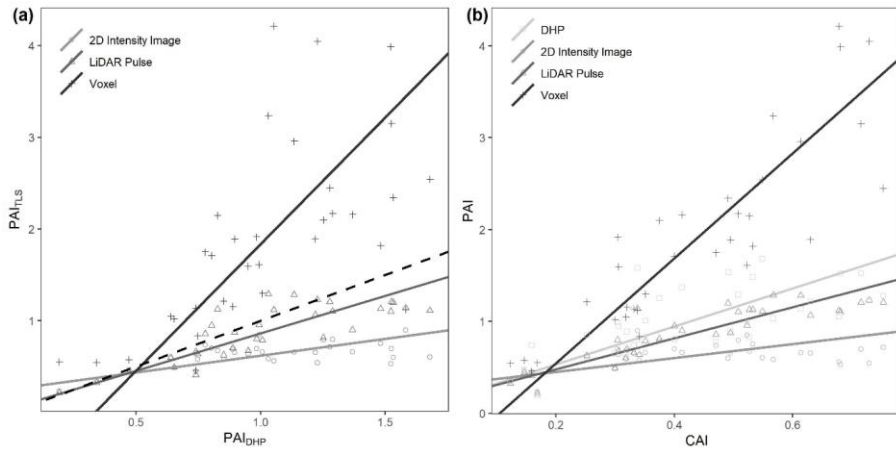
Formatted: Subscript

Formatted: Subscript

Formatted: Subscript

Formatted: Subscript

Formatted: Subscript



302

303 **Figure 4: Comparison of plot level $\text{TLS PAI PAI}_{\text{TLS}}$ and $\text{DHP PAI PAI}_{\text{DHP}}$, and CAI vs PAI estimates for all 33 plots. (a)**
 304 The correlation between DHP derived PAI and PAI derived using 2D Intensity Image $R^2 = 0.35$, slope = 0.36, $p < 0.01$,
 305 $\text{RMSE} = 0.39$ (circle), LiDAR Pulse $R^2 = 0.66$, slope = 0.82, $p < 0.01$, $\text{RMSE} = 0.14$ (triangle) and Voxel-Based $R^2 = 0.39$,
 306 slope = 2.76, $p < 0.01$, $\text{RMSE} = 0.88$ (cross) methods (b) The correlation between TLS derived CAI and PAI derived
 307 using DHP $R^2 = 0.46$, slope = 2.07, $p < 0.01$ (square), 2D Intensity Image $R^2 = 0.15$, slope = 0.76, $p < 0.05$ (circle) LiDAR
 308 Pulse $R^2 = 0.79$, slope = 1.69, $p < 0.01$ (triangle) and Voxel-Based $R^2 = 0.76$, slope = 5.72, $p < 0.01$ (cross) methods. Lines
 309 show statistically significant relationships fitted using SMA ($p < 0.01$). Dashed line in panel a represents 1:1 relationship.

310

311 3.4 Influence of species, tree height and CAI on α

312 To understand drivers of variance in α , we used individual tree PAI and WAI, calculated using the *Voxel-Based*
 313 method to test the relationship between species and α , and height/ CAI and α . We found that more drought tolerant
 314 species generally had higher α values than less drought tolerant species (Table A1; Figure 5), however, confidence
 315 intervals were wide and overlapping, suggesting that species is not a strong predictor of variation in α . We found
 316 a statistically significant negative effect of height ($p < 0.001$; Table A2; Figure 6a) and positive effect of CAI
 317 ($p < 0.01 - 0.05$; Table A2; Figure 6b) on α for all species apart from *P. sylvestris*. α decreased more rapidly with
 318 height and increased less rapidly with CAI for oaks than pines. Statistically significant ICC values were higher
 319 for *P. nigra* (ICC = 0.211; Table A2) than *P. pinaster*, *Q. faginea* and *Q. ilex* (ICC = 0.036; 0.060; 0.070,
 320 respectively), showing that more α variation is explained by the random plot effect in *P. nigra* than the other
 321 species. *P. pinaster* has a wider confidence interval (Figure 5), possibly explained by its lower sample size. [To](#)

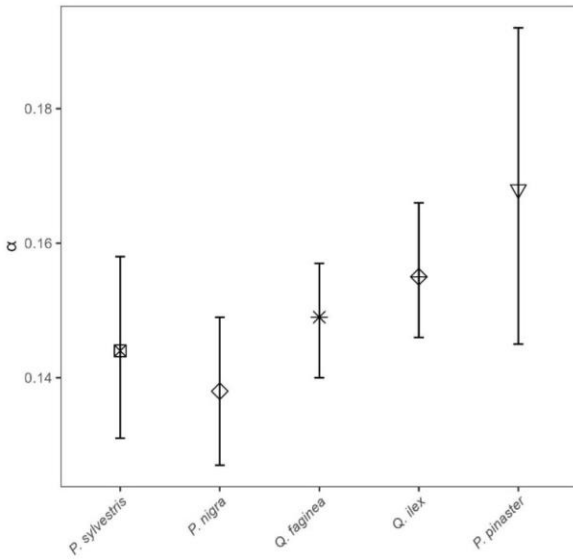
Formatted: Subscript

Formatted: Subscript

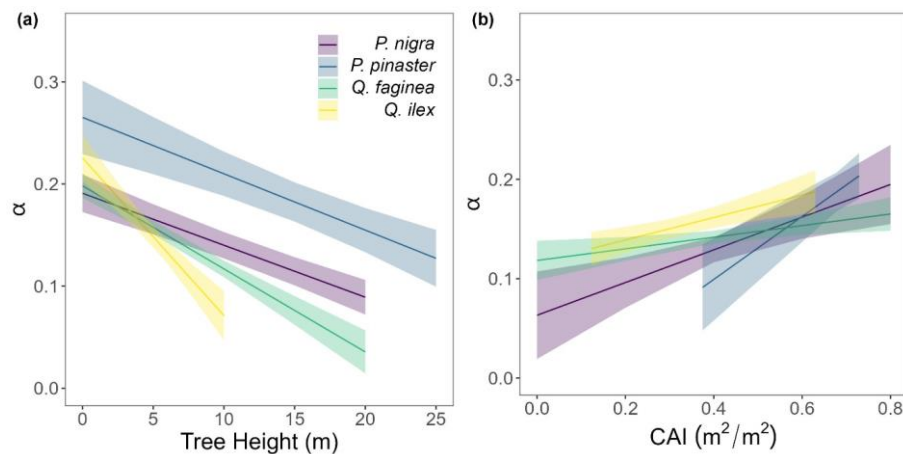
Formatted: Superscript

Formatted: Font: 7 pt

322 understand drivers of variance in WAI we carried out additional analysis to test the relationship between WAI
 323 and species, height, CAI and PAI, and presented these results in Appendix C.



324 **Figure 5:** Linear mixed model derived α values (a, equation 1) for all 2472 individual trees of species *P. sylvestris*, *P.*
 325 *nigra*, *Q. faginea*, *Q. ilex* and *P. pinaster*. Error bars represent 95% confidence intervals. Species are listed from low –
 326 high drought tolerance, with the exception of *P. pinaster*, for which drought tolerance index has not been calculated in
 327 the literature. [Drought tolerance rankings are taken from](#) Niinemets and Valladares, (2006)



328 **Figure 6:** Variation in α for each species: *Pinus nigra*, *P. pinaster*, *Q. faginea* and *Q. ilex* with (a) height and (b) plot
 329 CAI. Lines represent statistically significant linear mixed models (equation 2; $p < 0.001$ – $p < 0.05$). Ribbons represent
 330 95% confidence intervals. The model for *P. sylvestris* was not statistically significant.

331

332

333

334 **4. Discussion**

335 **4.1 Comparison of approaches to deriving PAI from remote sensed data**

336 We found substantial differences in PAI values estimated from TLS and DHP and from different TLS processing
337 methods (Figures 3 and 4). Further, differences between TLS methods varied across plot structure (CAI), with the
338 greatest differences between methods in plots with high CAI, and therefore high canopy density. Although
339 previous studies have presented TLS as an improvement over DHP due to its independence of illumination and
340 sky conditions during the data acquisition phase, and ability to resolve fine-scale canopy elements and gaps
341 (Calders et al., 2018; Grotti et al., 2020; Zhu et al., 2018), we have shown that there is large variability between
342 TLS processing methods in Mediterranean forests. Rigorous intercomparison of approaches, ideally using
343 standard benchmarking TLS datasets, and destructive sampling, would improve trust and reliability of TLS
344 algorithms.

345 **4.2 The LiDAR Pulse and 2D Intensity Image method derived PAI estimates were lower than those derived
346 from DHP and the Voxel-Based method**

347 We found the *LiDAR Pulse* method (Jupp et al., 2008) to have the best agreement with DHP for both whole plot
348 and single scan PAI estimates. In contrast to previous [studies comparing PAI_{TLS} with PAI_{DHP} comparisons](#)
349 (Calders et al., 2018; Grotti et al., 2020; Woodgate et al., 2015), we found that the *LiDAR Pulse* and *2D Intensity
350 Image* methods underestimated PAI compared to DHP, except at very low PAI values [\(PAI_{TLS} < 0.5\)](#).
351 Quantification of PAI from DHP may introduce additional sources of error, for example, its relatively lower
352 resolution compared to TLS could lead to mixed pixels that have a greater chance of misclassification of sky as
353 vegetation (Jonckheere et al., 2004). This effect could be enhanced in a Mediterranean forest as trees in drier
354 climates tend to have smaller leaves (Peppe et al., 2011), leading to more small canopy gaps that TLS may resolve
355 where DHP cannot. Further, although we took steps to reduce the error introduced at DHP data acquisition and
356 processing steps, including using automatic thresholding and collecting images with multiple exposures, DHP
357 processing requires both model and user assumptions that can impact results. For example, [DHP PAI PAI_{DHP}](#)
358 estimates are highly sensitive to camera exposure; increasing one stop of exposure can result in 3–28% difference
359 in PAI and use of automatic exposure can result in up to 70% error (Zhang et al., 2005).

Formatted: Subscript

Formatted: Subscript

Formatted: Subscript

Formatted: Subscript

360 We found the *Voxel-Based* method overestimated PAI values compared to the other methods at the whole plot
361 level. This is likely due to the method's use of co-registered scans, rather than averaged single scan PAI values,
362 since co-registered scans will reduce occlusion effects prevalent in single scan data that could lead to an
363 underestimation of PAI (Wilkes et al., 2017). The *Voxel-Based* method is, however, sensitive to voxel size (Li et
364 al., 2016), and larger voxels lead to larger PAI estimates as they fill small canopy gaps; we chose a voxel size of
365 0.05 m to match the minimum distance between points in our downsampled dataset. However, the *Voxel-Based*
366 method is a memory intensive approach to calculating PAI, and smaller voxels have higher memory requirements.
367 We picked this data resolution, and therefore voxel size, to balance the need to capture fine-scale canopy details
368 against memory requirements for running many large plots. Voxel size could have been chosen based on
369 estimates' match to DHP, but this would assume (1) that DHP estimates are most accurate, and (2) that DHP data
370 are always available, limiting the wider applicability of our findings. Understanding which method is over or
371 underestimating would require a destructively sampled dataset for validation, which was not possible for this

372 study (or most ecosystems). However, other studies using voxel approaches have found that although these
373 produce high LAI values for individual trees, these are underestimates compared with destructive samples (Li et
374 al., 2016). Regardless, PAI and LAI estimates using a *Voxel-Based* approach are highly dependent on voxel size
375 (Béland et al., 2014) (Li et al., 2016), and future work should test the influence of voxel size on PAI estimates,
376 using destructive samples in a range of environments.

377 **4.3 Relationship between PAI and CAI varied according to method and sensor**

378 The relationship between the LiDAR Pulse method had the strongest relationship (defined as highest R²) with and
379 TLS derived CAI had the highest R², demonstrating that the method is well suited to measuring PAI across the
380 range of plot CAI values used in this study. Although the *2D Intensity Image* method can tackle the significant
381 challenges presented by edge effects and partial beam interceptions, particularly present in phase-shift systems
382 (Grotti et al., 2020), our results suggest this method has a lower performance ability, with saturation occurring
383 sooner than all other methods in dense forests (Figures 3 and 4). The *2D Intensity Image* method uses the same
384 raw single scan data as the *LiDAR Pulse* method, so the better performance from the latter is likely due to the
385 method's use of vertically resolved gap fraction; both the *LiDAR Pulse* method and *Voxel-Based* method account
386 for the vertical structure of the canopy by summing vertical slices through the canopy.

387 **4.4 α variation between species and plot**

388 We used the *Voxel-Based* method to investigate individual tree α variation between species and across structure,
389 as this was the only approach we compared/identified that could be applied to single tree point clouds. We found
390 α values obtained were within the range of values obtained from destructive approaches (0.1 – 0.6, Gower et al.,
391 1997). The drought and shade intolerant *P. nigra* showed stronger variability in α across plots (higher ICC value,
392 Table A2) than other species, suggesting its wood – leaf ratio may be more sensitive to site factors. However, as
393 the plots measured in this study vary in both abiotic conditions (altitude, aspect, slope, wetness) as well as species
394 composition, stem density and canopy cover, there may be other drivers of variation in α values.

395 We found some evidence that species with higher drought tolerance had higher α values (Figure 5; Table A1),
396 however, confidence intervals were wide, suggesting a weak relationship. There is evidence that trees that tolerate
397 water limited environments have a lower leaf area (Battaglia et al., 1998; Mencuccini and Grace, 1995), so higher
398 α values may reflect maintenance of homeostasis of leaf water use through adjustment of wood to leaf area ratio
399 (Carter and White, 2009; Gazal et al., 2006). The potential for a tree to lose water is mostly regulated through leaf
400 traits including stomatal conductance and leaf area, and both stand (Battaglia et al., 1998; Specht and Specht,
401 1989) and individual tree (Mencuccini, 2003) water use have been found to scale linearly with LAI, with drought
402 often mitigated through leaf shedding (López et al., 2021).

403 **4.5 Tree stature and stand density drives α variation**

404 Although species had a weak relationship with explain some variation in α , tree height and plot CAI were stronger
405 predictor had a statistically significant relationship with α (p<0.001 – p<0.05) for all species, showing the
406 importance of local stand structure on leaf and woody allocation. We found that α scaled negatively with height
407 for all species apart from *P. sylvestris*, suggesting that in this environment, taller trees generally have a lower
408 proportion of wood to plant area index than shorter ones. *P. sylvestris*, which is at the edge of its geographical
409 range and physiological limits (Castro-Díez et al., 1997; Owen et al., 2021), showed no significant relationship

410 between height and α . We found that α scaled positively with plot level CAI for all species apart from *P. sylvestris*,
411 that is, trees growing in denser plots have a higher α . This supports theory that trees growing in dense forests are
412 competing for resources, reducing individual tree leaf area (Jump et al., 2017). The negative height – α and positive
413 CAI – α relationships in our model suggest that trees may initially invest in vertical growth to reach the canopy
414 level, and once there invest in lateral growth, with more leaf area, to increase light capture. This supports theory
415 that trees grow to outcompete neighbouring individuals for light capture (Purves and Pacala, 2008) and evidence
416 that both lateral growth and LAI are reduced beneath closed canopies (Beaudet and Messier, 1998; Canham,
417 1988).

418 Wood may be harder to accurately classify than leaves in TLS data (Vicari et al., 2019), resulting in a higher
419 occurrence of false positives in wood clouds, potentially leading to an overestimation in WAI, and therefore
420 underestimation of α , especially in trees with small leaves which are prevalent in dry, Mediterranean environments
421 (Peppe et al., 2011). The problem of misclassification will increase in taller trees due to TLS beam divergence,
422 occlusion and larger beam footprint at further distances (Vicari et al., 2019), suggesting that WAI overestimation
423 could be more pronounced in tall trees. Although our dense scanning strategy (Owen et al., 2021) was designed
424 to mitigate some of these effects, it is possible our findings could underestimate the slope of the negative
425 relationship between α and tree height.

426 **4.6 Correcting for non-photosynthetic elements in LAI estimates using TLS**

427 The value of TLS data to estimate individual tree PAI, WAI and subsequently α , demonstrates their potential to
428 corrective factors for non-photosynthetic components in ground based remote sensing measurements of LAI.
429 Properly correcting for WAI in LAI estimates is of global importance as small errors in ground based
430 measurements propagate through to large scale satellite observations generating large errors in global vegetation
431 models (Calders et al., 2018). [The work presented here provides a foundation for future work combining multi-source and multi-scale remote sensing datasets to correct large-scale LAI products](#). Our results echo others' in
432 finding that the prevalence of woody material in the tree canopy, and therefore α , is dynamic and varies by species
433 as well as senescence, crown health and, in the case of deciduous forests, leaf phenology (Gower et al., 1999).
434 The use of single α value in a plot or region (Olivas et al., 2013; Woodgate et al., 2016), invariant of species, size
435 and forest structure, to convert PAI to LAI is therefore problematic (Niu et al., 2021). Our study demonstrates the
436 importance of taking species mix and structural variation into account when correcting for non-photosynthetic
437 material in ground-based LAI estimates.

438 **5. Conclusions**

439 We tested three methods for estimating PAI using Terrestrial Laser Scanning data and compared these against
440 traditional DHP measurements. We found large variation between PAI values estimated from each TLS method
441 and DHP, demonstrating that care should be taken when deriving PAI from ground based remote sensing methods.
442 Although the *LiDAR Pulse* method was found to have the best agreement with both single scan and whole plot
443 PAI values measured by DHP, the *Voxel-Based* method allowed separate analysis of the key metric used to correct
444 for the effect of WAI in LAI measurements, α , in individual trees. We recommend the *LiDAR Pulse* method as a
445 fast and effective method for PAI estimation independent of illumination conditions. Whilst the *Voxel-Based*
446 method may be used to analyse individual tree α and determine ecological drivers of variation, work remains to

448 determine the validity of these approaches, in particular correct voxel size choice. We found that α varies by
449 species, height and stand density, showing the importance of accurately correcting for WAI on the individual tree
450 level and the utility of TLS to do so.

451 The variation in our results for the different methods used to derive PAI from TLS data show that there is some
452 way to go before TLS derived vegetation indices can be interpreted as robust and reliable. Validation using
453 destructive samples and further intercomparison studies of methods are needed to demonstrate the advantages of
454 TLS, and use of benchmarking datasets should be standard. DHP is a faster, cheaper and more widely accessible
455 method for PAI estimation, and while TLS promises to alleviate potential bias in DHP estimates, results are highly
456 methods dependent. Our results demonstrate the challenges that stand in the way of large scale adoption of TLS
457 for vegetation indices monitoring.

458 **6. Code availability**

459 See https://github.com/will-flynn/tls_dhp_pai.git for all processing and modelling code.

460 **7. Data availability**

461 See Owen et al., (2022) for individual segmented tree data.

462 **8. Author contribution**

463 All authors designed the study. HJFO and WRMF collected and processed TLS and DHP data; WRMF performed
464 formal analysis with guidance from all authors. WRMF led the writing with input from all authors. All authors
465 contributed critically to drafts and gave final approval for publication.

466 **9. Competing interests**

467 The authors declare that they have no conflict of interest.

468 **7. Acknowledgements**

469 WRMF was funded through a London NERC DTP PhD studentship. ERL, HJFO and SWDG were funded through
470 the UKRI Future Leaders Fellowship awarded to ERL (MR/T019832/1).

471 **References**

472 Baeten, L., Verheyen, K., Wirth, C., Bruelheide, H., Bussotti, F., Finér, L., Jaroszewicz, B., Selvi, F.,
473 Valladares, F., Allan, E., Ampoorter, E., Auge, H., Avăcărei, D., Barbaro, L., Bărnăicea, I., Bastias, C. C.,
474 Bauhus, J., Beinhoff, C., Benavides, R., Benneter, A., Berger, S., Berthold, F., Boberg, J., Bonal, D.,
475 Brüggemann, W., Carnol, M., Castagneyrol, B., Charbonnier, Y., Chekko, E., Coomes, D., Coppi, A., Dalmaris,
476 E., Dănilă, G., Dawud, S. M., de Vries, W., De Wandeler, H., Deconchat, M., Domisch, T., Duduman, G.,
477 Fischer, M., Fotelli, M., Gessler, A., Gimeno, T. E., Granier, A., Grossiord, C., Guyot, V., Hantsch, L.,
478 Hättenschwiler, S., Hector, A., Hermy, M., Holland, V., Jactel, H., Joly, F.-X., Jucker, T., Kolb, S., Koricheva,
479 J., Lexer, M. J., Liebergesell, M., Milligan, H., Müller, S., Muys, B., Nguyen, D., Nichiforel, L., Pollastrini, M.,
480 Proulx, R., Rabasa, S., Radoglou, K., Ratcliffe, S., Raulund-Rasmussen, K., Seiferling, I., Stenlid, J., Vesterdal,
481 L., von Wilpert, K., Zavala, M. A., Zielinski, D., and Scherer-Lorenzen, M.: A novel comparative research
482 platform designed to determine the functional significance of tree species diversity in European forests,
483 *Persepect. Plant. Ecol.*, 15, 281–291, <https://doi.org/10.1016/j.ppees.2013.07.002>, 2013.

484 Baret, F., Weiss, M., Lacaze, R., Camacho, F., Makhmara, H., Pacholczyk, P., and Smets, B.: GEOV1: LAI and
485 FAPAR essential climate variables and FCOVER global time series capitalizing over existing products. Part1:
486 Principles of development and production, *Remote Sens. Environ.*, 137, 299–309,
487 <https://doi.org/10.1016/j.rse.2012.12.027>, 2013.

488 Bates, D., Mächler, M., Bolker, B., and Walker, S.: Fitting Linear Mixed-Effects Models Using lme4, *J. Stat. Softw.*, 67, <https://doi.org/10.18637/jss.v067.i01>, 2015.

490 Battaglia, M., Cherry, M. L., Beadle, C. L., Sands, P. J., and Hingston, A.: Prediction of leaf area index in
491 eucalypt plantations: effects of water stress and temperature, *Tree Physiol.*, 18, 521–528,
492 <https://doi.org/10.1093/treephys/18.8-9.521>, 1998.

493 Beaudet, M. and Messier, C.: Growth and morphological responses of yellow birch, sugar maple, and beech
494 seedlings growing under a natural light gradient, *Can. J. Forest Res.*, 28, 1007–1015,
495 <https://doi.org/10.1139/x98-077>, 1998.

496 Béland, M., Baldocchi, D. D., Widlowski, J.-L., Fournier, R. A., and Verstraete, M. M.: On seeing the wood
497 from the leaves and the role of voxel size in determining leaf area distribution of forests with terrestrial LiDAR,
498 *Agr. Forest Meterol.*, 184, 82–97, <https://doi.org/10.1016/j.agrformet.2013.09.005>, 2014.

499 Breda, N. J. J.: Ground-based measurements of leaf area index: a review of methods, instruments and current
500 controversies, *J. Exp. Bot.*, 54, 2403–2417, <https://doi.org/10.1093/jxb/erg263>, 2003.

501 Burt, A., Disney, M., and Calders, K.: Extracting individual trees from lidar point clouds using treeseg, *Methods Ecol. Evol.*, 10, 438–445, <https://doi.org/10.1111/2041-210X.13121>, 2019.

502 Calders, K., Armston, J., Newnham, G., Herold, M., and Goodwin, N.: Implications of sensor configuration and
503 topography on vertical plant profiles derived from terrestrial LiDAR, *Agr. Forest Meterol.*, 194, 104–117,
504 <https://doi.org/10.1016/j.agrformet.2014.03.022>, 2014.

505 Calders, K., Origo, N., Disney, M., Nightingale, J., Woodgate, W., Armston, J., and Lewis, P.: Variability and
506 bias in active and passive ground-based measurements of effective plant, wood and leaf area index, *Agr. Forest
507 Meterol.*, 252, 231–240, <https://doi.org/10.1016/j.agrformet.2018.01.029>, 2018.

508 Calders, K., Adams, J., Armston, J., Bartholomeus, H., Bauwens, S., Bentley, L. P., Chave, J., Danson, F. M.,
509 Demol, M., Disney, M., Gaulton, R., Krishna Moorthy, S. M., Levick, S. R., Saarinen, N., Schaaf, C., Stovall,
510 A., Terryn, L., Wilkes, P., and Verbeeck, H.: Terrestrial laser scanning in forest ecology: Expanding the
511 horizon, *Remote Sensing of Environment*, 251, 112102, <https://doi.org/10.1016/j.rse.2020.112102>, 2020.

512 Canham, C. D.: Growth and Canopy Architecture of Shade-Tolerant Trees: Response to Canopy Gaps, *Ecology*,
513 69, 786–795, <https://doi.org/10.2307/1941027>, 1988.

514 Carter, J. L. and White, D. A.: Plasticity in the Huber value contributes to homeostasis in leaf water relations of
515 a mallee Eucalypt with variation to groundwater depth, *Tree Physiol.*, 29, 1407–1418,
516 <https://doi.org/10.1093/treephys/tp076>, 2009.

517 Caspersen, J. P., Vanderwel, M. C., Cole, W. G., and Purves, D. W.: How Stand Productivity Results from Size-
518 and Competition-Dependent Growth and Mortality, *PLoS ONE*, 6, e28660,
519 <https://doi.org/10.1371/journal.pone.0028660>, 2011.

520 Castro-Díez, P., Villar-Salvador, P., Pérez-Rontomé, C., Maestro-Martínez, M., and Montserrat-Martí, G.: Leaf
521 morphology and leaf chemical composition in three *Quercus* (Fagaceae) species along a rainfall gradient in NE
522 Spain, *Trees*, 11, 127–134, <https://doi.org/10.1007/PL00009662>, 1997.

523 Chen, J. M. and Black, T. A.: Defining leaf area index for non-flat leaves, *Plant Cell Environ.*, 15, 421–429,
524 <https://doi.org/10.1111/j.1365-3040.1992.tb00992.x>, 1992.

525 Coomes, D. A., Holdaway, R. J., Kobe, R. K., Lines, E. R., and Allen, R. B.: A general integrative framework
526 for modelling woody biomass production and carbon sequestration rates in forests, *Journal of Ecology*, 100, 42–
527 64, <https://doi.org/10.1111/j.1365-2745.2011.01920.x>, 2012.

528 Disney, M.: Terrestrial LiDAR: a three-dimensional revolution in how we look at trees, *New Phytol.*, 222,
529 1736–1741, <https://doi.org/10.1111/nph.15517>, 2018.

530

531 Gazal, R. M., Scott, R. L., Goodrich, D. C., and Williams, D. G.: Controls on transpiration in a semiarid riparian
532 cottonwood forest, *Agr. Forest Meterol.*, 137, 56–67, <https://doi.org/10.1016/j.agrformet.2006.03.002>, 2006.

533 Gower, S. T., Vogel, J. G., Norman, J. M., Kucharik, C. J., Steele, S. J., and Stow, T. K.: Carbon distribution
534 and aboveground net primary production in aspen, jack pine, and black spruce stands in Saskatchewan and
535 Manitoba, Canada, *J. Geophys. Res.*, 102, 29029–29041, <https://doi.org/10.1029/97JD02317>, 1997.

536 Gower, S. T., Kucharik, C. J., and Norman, J. M.: Direct and Indirect Estimation of Leaf Area Index, fAPAR,
537 and Net Primary Production of Terrestrial Ecosystems, *Remote Sens. Environ.*, 70, 29–51,
538 [https://doi.org/10.1016/S0034-4257\(99\)00056-5](https://doi.org/10.1016/S0034-4257(99)00056-5), 1999.

539 Grott, M., Calders, K., Origo, N., Puletti, N., Alivermini, A., Ferrara, C., and Chianucci, F.: An intensity, image-
540 based method to estimate gap fraction, canopy openness and effective leaf area index from phase-shift terrestrial
541 laser scanning, *Agr. Forest Meterol.*, 280, 107766, <https://doi.org/10.1016/j.agrformet.2019.107766>, 2020.

542 Hardwick, S. R., Toumi, R., Pfeifer, M., Turner, E. C., Nilus, R., and Ewers, R. M.: The relationship between
543 leaf area index and microclimate in tropical forest and oil palm plantation: Forest disturbance drives changes in
544 microclimate, *Agr. Forest Meterol.*, 201, 187–195, <https://doi.org/10.1016/j.agrformet.2014.11.010>, 2015.

545 Hijmans, R. J.: raster: Geographic Data Analysis and Modeling R package version 3.5-21, <https://CRAN.R-project.org/package=raster>., 2022.

546 Hosoi, F. and Omasa, K.: Voxel-Based 3-D Modeling of Individual Trees for Estimating Leaf Area Density
547 Using High-Resolution Portable Scanning Lidar, *IEEE T. Geosci. Remote*, 44, 3610–3618,
548 <https://doi.org/10.1109/TGRS.2006.881743>, 2006.

549 Itakura, K. and Hosoi, F.: Voxel-based leaf area estimation from three-dimensional plant images, *J. Agric.
550 Meteorol.*, 75, 211–216, <https://doi.org/10.2480/agrmet.d-19-00013>, 2019.

551 Jonckheere, I., Fleck, S., Nackaerts, K., Muys, B., Coppin, P., Weiss, M., and Baret, F.: Review of methods for
552 in situ leaf area index determination, *Agr. Forest Meterol.*, 121, 19–35,
553 <https://doi.org/10.1016/j.agrformet.2003.08.027>, 2004.

554 Jonckheere, I. G. C., Muys, B., and Coppin, P.: Allometry and evaluation of in situ optical LAI determination in
555 Scots pine: a case study in Belgium, *Tree Physiol.*, 25, 723–732, <https://doi.org/10.1093/treephys/25.6.723>,
556 2005.

557 Jucker, T., Bouriaud, O., Avacaritei, D., Dănilă, I., Duduman, G., Valladares, F., and Coomes, D. A.:
558 Competition for light and water play contrasting roles in driving diversity-productivity relationships in Iberian
559 forests, *J. Ecol.*, 102, 1202–1213, <https://doi.org/10.1111/1365-2745.12276>, 2014.

560 Jump, A. S., Ruiz-Benito, P., Greenwood, S., Allen, C. D., Kitzberger, T., Fensham, R., Martínez-Vilalta, J.,
561 and Lloret, F.: Structural overshoot of tree growth with climate variability and the global spectrum of drought-
562 induced forest dieback, *Glob. Change Biol.*, 23, 3742–3757, <https://doi.org/10.1111/gcb.13636>, 2017.

563 Jupp, D. L. B., Culvenor, D. S., Lovell, J. L., Newnham, G. J., Strahler, A. H., and Woodcock, C. E.: Estimating
564 forest LAI profiles and structural parameters using a ground-based laser called 'Echidna(R)', *Tree Physiol.*, 29,
565 171–181, <https://doi.org/10.1093/treephys/tpn022>, 2008.

566 Kamoske, A. G., Dahlin, K. M., Stark, S. C., and Serbin, S. P.: Leaf area density from airborne LiDAR:
567 Comparing sensors and resolutions in a temperate broadleaf forest ecosystem, *Forest Ecol. Manag.*, 433, 364–
568 375, <https://doi.org/10.1016/j.foreco.2018.11.017>, 2019.

569 Kuusk, V., Niinemets, Ü., and Valladares, F.: A major trade-off between structural and photosynthetic
570 investments operative across plant and needle ages in three Mediterranean pines, *Tree Physiol.*, 38, 543–557,
571 <https://doi.org/10.1093/treephys/tpx139>, 2018.

572 Leblanc, S. G. and Chen, J. M.: A practical scheme for correcting multiple scattering effects on optical LAI
573 measurements, *Agr. Forest Meterol.*, 110, 125–139, [https://doi.org/10.1016/S0168-1923\(01\)00284-2](https://doi.org/10.1016/S0168-1923(01)00284-2), 2001.

575 Lecigne, B., Delagrange, S., and Messier, C.: Exploring trees in three dimensions: VoxR, a novel voxel-based R
576 package dedicated to analysing the complex arrangement of tree crowns, *Ann. Bot-London*, 121, 589–601,
577 <https://doi.org/10.1093/aob/mcx095>, 2018.

578 Li, S., Dai, L., Wang, H., Wang, Y., He, Z., and Lin, S.: Estimating Leaf Area Density of Individual Trees
579 Using the Point Cloud Segmentation of Terrestrial LiDAR Data and a Voxel-Based Model, *Remote Sens-Basel*,
580 9, 1202, <https://doi.org/10.3390/rs9111202>, 2017.

581 Li, Y., Guo, Q., Tao, S., Zheng, G., Zhao, K., Xue, B., and Su, Y.: Derivation, Validation, and Sensitivity
582 Analysis of Terrestrial Laser Scanning-Based Leaf Area Index, *Can. J. Remote Sens.*, 42, 719–729,
583 <https://doi.org/10.1080/07038992.2016.1220829>, 2016.

584 Lines, E. R., Fischer, F. J., Owen, H. J. F., and Jucker, T.: The shape of trees: Reimagining forest ecology in
585 three dimensions with remote sensing, *J. Ecol.*, 110, 1730–1745, <https://doi.org/10.1111/1365-2745.13944>,
586 2022.

587 Long, J. N. and Smith, F. W.: Leaf area - sapwood area relations of lodgepole pine as influenced by stand
588 density and site index., *Can. J. Forest Res.*, 18, 247–250, 1988.

589 López, R., Cano, F. J., Martin-StPaul, N. K., Cochard, H., and Choat, B.: Coordination of stem and leaf traits
590 define different strategies to regulate water loss and tolerance ranges to aridity, *New Phytol.*, 230, 497–509,
591 <https://doi.org/10.1111/nph.17185>, 2021.

592 Lovell, J. L., Jupp, D. L. B., van Gorsel, E., Jimenez-Berni, J., Hopkinson, C., and Chasmer, L.: Foliage Profiles
593 from Ground Based Waveform and Discrete Point Lidar, *SilviLaser*, 1–9, 2011.

594 Ma, L., Zheng, G., Eitel, J. U. H., Magney, T. S., and Moskal, L. M.: Determining woody-to-total area ratio
595 using terrestrial laser scanning (TLS), *Agr. Forest Meterol.*, 228–229, 217–228,
596 <https://doi.org/10.1016/j.agrformet.2016.06.021>, 2016.

597 Madrigal-González, J., Herrero, A., Ruiz-Benito, P., and Zavala, M. A.: Resilience to drought in a dry forest:
598 Insights from demographic rates, *Forest Ecol. Manag.*, 389, 167–175,
599 <https://doi.org/10.1016/j.foreco.2016.12.012>, 2017.

600 Magnani, F., Mencuccini, M., and Grace, J.: Age-related decline in stand productivity: the role of structural
601 acclimation under hydraulic constraints, *Plant Cell Environ.*, 23, 251–263, <https://doi.org/10.1046/j.1365-3040.2000.00537.x>, 2000.

603 Mencuccini, M.: The ecological significance of long-distance water transport: short-term regulation, long-term
604 acclimation and the hydraulic costs of stature across plant life forms, *Plant Cell Environ.*, 26, 163–182,
605 <https://doi.org/10.1046/j.1365-3040.2003.00991.x>, 2003.

606 Mencuccini, M. and Grace, J.: Climate influences the leaf area/sapwood area ratio in Scots pine, *Tree Physiol.*,
607 15, 1–10, <https://doi.org/10.1093/treephys/15.1.1>, 1995.

608 Monsi, M. and Saeki, T.: On the Factor Light in Plant Communities and its Importance for Matter Production,
609 *Ann. Bot-London*, 95, 549–567, <https://doi.org/10.1093/aob/mci052>, 1953.

610 Nakagawa, S., Johnson, P. C. D., and Schielzeth, H.: The coefficient of determination R² and intra-class
611 correlation coefficient from generalized linear mixed-effects models revisited and expanded, *J. R. Soc.
612 Interface*, 14, 20170213, <https://doi.org/10.1098/rsif.2017.0213>, 2017.

613 Niinemets, Ü. and Valladares, F.: Tolerance to shade, drought, and waterlogging of temperate northern
614 hemisphere trees and shrubs, *Ecol. Monogr.*, 76, 521–547, [https://doi.org/10.1890/0012-9615\(2006\)076\[0521:TTSDAW\]2.0.CO;2](https://doi.org/10.1890/0012-9615(2006)076[0521:TTSDAW]2.0.CO;2), 2006.

616 Niu, X., Fan, J., Luo, R., Fu, W., Yuan, H., and Du, M.: Continuous estimation of leaf area index and the
617 woody-to-total area ratio of two deciduous shrub canopies using fisheye webcams in a semiarid loessial region
618 of China, *Ecol. Indic.*, 125, 107549, <https://doi.org/10.1016/j.ecolind.2021.107549>, 2021.

619 Olivas, P. C., Oberbauer, S. F., Clark, D. B., Clark, D. A., Ryan, M. G., O'Brien, J. J., and Ordoñez, H.:
620 Comparison of direct and indirect methods for assessing leaf area index across a tropical rain forest landscape,
621 *Agr. Forest Meterol.*, 177, 110–116, <https://doi.org/10.1016/j.agrformet.2013.04.010>, 2013.

622 Owen, H. J. F., Flynn, W. R. M., and Lines, E. R.: Competitive drivers of inter-specific deviations of crown
623 morphology from theoretical predictions measured with Terrestrial Laser Scanning, *J. Ecol.*, 109, 2612–2628,
624 <https://doi.org/10.1111/1365-2745.13670>, 2021.

625 Owen, H. J. F., Flynn, W. R. M., and Lines, E. R.: Individual TLS tree clouds collected from both Alto Tajo and
626 Cuellar in Spain., [10.5281/zenodo.6962717](https://doi.org/10.5281/zenodo.6962717), 2022.

627 Peppe, D. J., Royer, D. L., Cariglino, B., Oliver, S. Y., Newman, S., Leight, E., Enikolopov, G., Fernandez-
628 Burgos, M., Herrera, F., Adams, J. M., Correa, E., Currano, E. D., Erickson, J. M., Hinojosa, L. F., Hoganson, J.
629 W., Iglesias, A., Jaramillo, C. A., Johnson, K. R., Jordan, G. J., Kraft, N. J. B., Lovelock, E. C., Lusk, C. H.,
630 Niinemets, Ü., Peñuelas, J., Rapson, G., Wing, S. L., and Wright, I. J.: Sensitivity of leaf size and shape to
631 climate: global patterns and paleoclimatic applications, *New Phytol.*, 190, 724–739,
632 <https://doi.org/10.1111/j.1469-8137.2010.03615.x>, 2011.

633 Pfeifer, M., Gonsamo, A., Disney, M., Pellikka, P., and Marchant, R.: Leaf area index for biomes of the Eastern
634 Arc Mountains: Landsat and SPOT observations along precipitation and altitude gradients, *Remote Sens.*
635 *Environ.*, 118, 103–115, <https://doi.org/10.1016/j.rse.2011.11.009>, 2012.

636 Phillips, N., Bond, B. J., McDowell, N. G., Ryan, M. G., and Schauer, A.: Leaf area compounds height-related
637 hydraulic costs of water transport in Oregon White Oak trees, *Funct. Ecol.*, 17, 832–840,
638 <https://doi.org/10.1111/j.1365-2435.2003.00791.x>, 2003.

639 Purves, D. and Pacala, S.: Predictive Models of Forest Dynamics, *Science*, 320, 1452–1453,
640 <https://doi.org/10.1126/science.1155359>, 2008.

641 Ridler, T. W. and Calvard, S.: Picture Thresholding Using an Iterative Selection Method, *IEEE T. Syst. Man.*
642 *Cyb.*, 8, 630–632, <https://doi.org/10.1109/TSMC.1978.4310039>, 1978.

643 Sea, W. B., Choler, P., Beringer, J., Weinmann, R. A., Hutley, L. B., and Leuning, R.: Documenting
644 improvement in leaf area index estimates from MODIS using hemispherical photos for Australian savannas,
645 *Agr. Forest Meterol.*, 151, 1453–1461, <https://doi.org/10.1016/j.agrformet.2010.12.006>, 2011.

646 Specht, R. L. and Specht, A.: Canopy structure in Eucalyptus-dominated communities in Australia along
647 climatic gradients, *Canopy structure in Eucalyptus-dominated communities in Australia along climatic*
648 gradients, 10, 191–213, 1989.

649 Vicari, M. B., Disney, M., Wilkes, P., Burt, A., Calders, K., and Woodgate, W.: Leaf and wood classification
650 framework for terrestrial LiDAR point clouds, *Methods Ecol. Evol.*, 10, 680–694, <https://doi.org/10.1111/2041-210X.13144>, 2019.

652 Warton, D. I., Wright, I. J., Falster, D. S., and Westoby, M.: Bivariate line-fitting methods for allometry, *Biol.*
653 *Rev.*, 81, 259–291, <https://doi.org/10.1017/S1464793106007007>, 2006.

654 Warton, D. I., Duursma, R. A., Falster, D. S., and Taskinen, S.: smatr 3 - an R package for estimation and
655 inference about allometric lines: *The smatr 3 - an R package*, *Methods Ecol. Evol.*, 3, 257–259,
656 <https://doi.org/10.1111/j.2041-210X.2011.00153.x>, 2012.

657 Weiss, M., Baret, F., Smith, G. J., Jonckheere, I., and Coppin, P.: Review of methods for in situ leaf area index
658 (LAI) determination, *Agr. Forest Meterol.*, 121, 37–53, <https://doi.org/10.1016/j.agrformet.2003.08.001>, 2004.

660 Whitehead, D.: The Estimation of Foliage Area from Sapwood Basal Area in Scots Pine, *Forestry*, 51, 137–149,
661 <https://doi.org/10.1093/forestry/51.2.137>, 1978.

662 Wilkes, P., Lau, A., Disney, M., Calders, K., Burt, A., Gonzalez de Tanago, J., Bartholomeus, H., Brede, B., and
663 Herold, M.: Data acquisition considerations for Terrestrial Laser Scanning of forest plots, *Remote Sensing of*
664 *Environment*, 196, 140–153, <https://doi.org/10.1016/j.rse.2017.04.030>, 2017.

664 Woodgate, W., Jones, S. D., Suarez, L., Hill, M. J., Armston, J. D., Wilkes, P., Soto-Berelov, M., Haywood, A.,
665 and Mellor, A.: Understanding the variability in ground-based methods for retrieving canopy openness, gap
666 fraction, and leaf area index in diverse forest systems, *Agr. Forest Meterol.*, 205, 83–95,
667 <https://doi.org/10.1016/j.agrformet.2015.02.012>, 2015.

668 Woodgate, W., Armston, J. D., Disney, M., Jones, S. D., Suarez, L., Hill, M. J., Wilkes, P., and Soto-Berelov,
669 M.: Quantifying the impact of woody material on leaf area index estimation from hemispherical photography
670 using 3D canopy simulations, *Agr. Forest Meterol.*, 226–227, 1–12,
671 <https://doi.org/10.1016/j.agrformet.2016.05.009>, 2016.

672 Zhang, Y., Chen, J. M., and Miller, J. R.: Determining digital hemispherical photograph exposure for leaf area
673 index estimation, *Agr. Forest Meterol.*, 133, 166–181, <https://doi.org/10.1016/j.agrformet.2005.09.009>, 2005.

674 Zheng, G., Moskal, L. M., and Kim, S.-H.: Retrieval of Effective Leaf Area Index in Heterogeneous Forests
675 With Terrestrial Laser Scanning, *IEEE T. Geosci. Remote*, 51, 777–786,
676 <https://doi.org/10.1109/TGRS.2012.2205003>, 2013.

677 Zhu, X., Skidmore, A. K., Wang, T., Liu, J., Darvishzadeh, R., Shi, Y., Premier, J., and Heurich, M.: Improving
678 leaf area index (LAI) estimation by correcting for clumping and woody effects using terrestrial laser scanning,
679 *Agr. Forest Meterol.*, 263, 276–286, <https://doi.org/10.1016/j.agrformet.2018.08.026>, 2018.

680

Formatted

Appendix A

Table 1: species – α linear mixed model (equation 1) showing relationship between tree species and α for all 2472 individual trees. Species are listed from low – high drought tolerance, with the exception of *P. pinaster*, for which drought tolerance index has not been calculated in the literature.

Species	α (eq. 1)	95% CI
<i>P. sylvestris</i>	0.144	0.131, 0.158
<i>P. nigra</i>	0.138	0.127, 0.149
<i>Q. faginea</i>	0.149	0.140, 0.157
<i>Q. ilex</i>	0.155	0.146, 0.166
<i>P. pinaster</i>	0.168	0.145, 0.192

Table 2: height – α linear mixed models for each species (equation 2) showing relationship between tree height and plot CAI and α for all 2472 individual trees. Species are listed from low – high estimated α . Significance codes: p < 0.001 ‘***’; p < 0.01 ‘**’; p < 0.05 ‘*’; not significant ‘ns’

Species	b (eq. 2) (95% CI)	c (eq. 2) (95% CI)	ICC
<i>P. sylvestris</i>	-0.002 ^{ns} (-0.004, 0.000)	0.134 ^{ns} (0.010 0.259)	0.151
<i>P. nigra</i>	-0.005*** (-0.006, -0.004)	0.164** (0.063, 0.263)	0.211
<i>Q. faginea</i>	-0.008*** (-0.010, -0.007)	0.058* (0.016, 0.101)	0.060
<i>Q. ilex</i>	-0.015*** (-0.020, -0.011)	0.113** (0.050, 0.179)	0.070
<i>P. pinaster</i>	-0.006*** (-0.008, -0.004)	0.317* (0.177, 0.453)	0.036

Appendix B

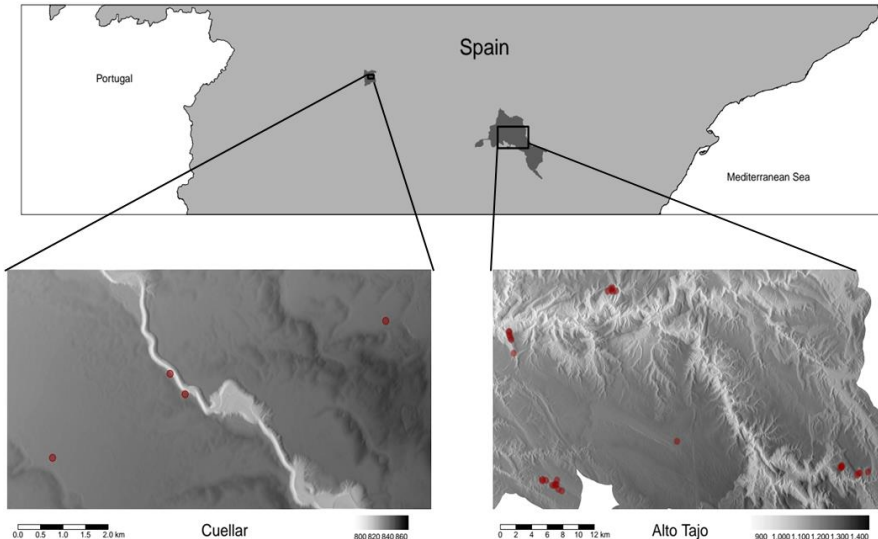


Figure 1: Map of plot locations within two field sites in central Spain (Cuellar, left and Alto Tajo, right). Red points show plot locations on high-resolution digital terrain models enhanced with hillshading shown in greyscale.

Appendix C

$$WAI = m_{species} + b \quad (1)$$

$$WAI = m_{height} + b \quad (2)$$

$$WAI = m_{CAI} + b \quad (3)$$

$$WAI = m_{PAI} + b \quad (4)$$

Where WAI is the wood area index, *species*, *height*, *CAI* and *PAI* are the tree species, tree height, crown area index of the plot in which the tree is growing and tree plant area index respectively and *m* and *b* are parameters to be fit.

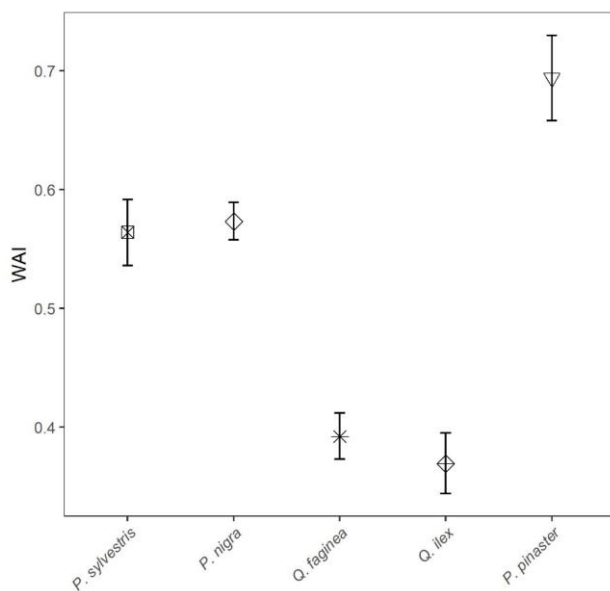


Figure 2: Linear model derived WAI values (m, equation C1) for all 2472 individual trees of species *P. sylvestris*, *P. nigra*, *Q. faginea*, *Q. ilex* and *P. pinaster*. Error bars represent 95% confidence intervals. Species are listed from low – high drought tolerance, with the exception of *P. pinaster*, for which drought tolerance index has not been calculated in the literature.

Table 3: Linear model (equation C1) showing relationship between tree species and WAI for all 2471 individual trees. Significance codes: $p < 0.001$ ****; $p < 0.01$ **; $p < 0.05$ *; not significant ns

Species	<i>m</i> (eq. 1)	Std. Error	P value
<i>P. nigra</i>	0.57	0.008	***
<i>P. pinaster</i>	0.69	0.018	
<i>P. sylvestris</i>	0.56	0.014	
<i>Q. faginea</i>	0.39	0.010	***
<i>Q. ilex</i>	0.37	0.013	***

Table 4: Linear models (equations C2, C3, C4) predicting WAI as a function of tree height, CAI (density) and PAI
 Significance codes: p < 0.001 ‘***’; p < 0.01 ‘**’; p < 0.05 ‘*’; not significant ‘ns’

	<i>m</i> (eq. 2, 3, 4)	R ²	P value
Tree Height	0.02	0.27	***
CAI	0.39	0.78	***
PAI	0.11	0.35	***